

Review

# Early Diagnosis of Neurodegenerative Diseases: What Has Been Undertaken to Promote the Transition from PET to Fluorescence Tracers

Nicolò Bisi <sup>1,\*</sup>, Luca Pinzi <sup>2</sup> , Giulio Rastelli <sup>2</sup>  and Nicolò Tonali <sup>1,\*</sup> <sup>1</sup> Université Paris-Saclay, CNRS, BioCIS, Bat. Henri Moissan, 17, Av. des Sciences, 91400 Orsay, France<sup>2</sup> Department of Life Sciences, University of Modena and Reggio Emilia, Via Giuseppe Campi 103, 41125 Modena, Italy; luca.pinzi@unimore.it (L.P.); giulio.rastelli@unimore.it (G.R.)

\* Correspondence: bisinicolo@gmail.com (N.B.); nicolo.tonali@universite-paris-saclay.fr (N.T.)

**Abstract:** Alzheimer's Disease (AD) and Parkinson's Disease (PD) represent two among the most frequent neurodegenerative diseases worldwide. A common hallmark of these pathologies is the misfolding and consequent aggregation of amyloid proteins into soluble oligomers and insoluble  $\beta$ -sheet-rich fibrils, which ultimately lead to neurotoxicity and cell death. After a hundred years of research on the subject, this is the only reliable histopathological feature in our hands. Since AD and PD are diagnosed only once neuronal death and the first symptoms have appeared, the early detection of these diseases is currently impossible. At present, there is no effective drug available, and patients are left with symptomatic and inconclusive therapies. Several reasons could be associated with the lack of effective therapeutic treatments. One of the most important factors is the lack of selective probes capable of detecting, as early as possible, the most toxic amyloid species involved in the onset of these pathologies. In this regard, chemical probes able to detect and distinguish among different amyloid aggregates are urgently needed. In this article, we will review and put into perspective results from ex vivo and in vivo studies performed on compounds specifically interacting with such early species. Following a general overview on the three different amyloid proteins leading to insoluble  $\beta$ -sheet-rich amyloid deposits (amyloid  $\beta_{1-42}$  peptide, Tau, and  $\alpha$ -synuclein), a list of the advantages and disadvantages of the approaches employed to date is discussed, with particular attention paid to the translation of fluorescence imaging into clinical applications. Furthermore, we also discuss how the progress achieved in detecting the amyloids of one neurodegenerative disease could be leveraged for research into another amyloidosis. As evidenced by a critical analysis of the state of the art, substantial work still needs to be conducted. Indeed, the early diagnosis of neurodegenerative diseases is a priority, and we believe that this review could be a useful tool for better investigating this field.

**Keywords:**  $A\beta_{1-42}$ ; Tau;  $\alpha$ -synuclein; probes; neurodegeneration; Alzheimer's disease; Parkinson's disease; tauopathies



**Citation:** Bisi, N.; Pinzi, L.; Rastelli, G.; Tonali, N. Early Diagnosis of Neurodegenerative Diseases: What Has Been Undertaken to Promote the Transition from PET to Fluorescence Tracers. *Molecules* **2024**, *29*, 722. <https://doi.org/10.3390/molecules29030722>

Academic Editor: Krishan Kumar

Received: 4 January 2024

Revised: 29 January 2024

Accepted: 30 January 2024

Published: 4 February 2024



**Copyright:** © 2024 by the authors. Licensee MDPI, Basel, Switzerland. This article is an open access article distributed under the terms and conditions of the Creative Commons Attribution (CC BY) license (<https://creativecommons.org/licenses/by/4.0/>).

## 1. Introduction

Neurodegenerative diseases represent one of the main causes of public health concerns to date, affecting almost 179 million people worldwide and costing more than EUR 800 billion only in Europe [1]. Alzheimer's Disease (AD) and Parkinson's Disease (PD) are the first and the second most common neurodegenerative diseases, respectively, both of them being amyloidopathies in which an amyloid protein misfolds and aggregates, causing neurotoxicity and cell death [2]. In the case of AD, the amyloids involved are tubulin associated unit (Tau) and  $A\beta_{1-42}$ , while in PD,  $\alpha$ -synuclein ( $\alpha$ Syn) is the one whose misfolding and aggregation leads to toxic inclusions and neuronal death. Throughout the preceding century, researchers endeavored to elucidate the primary pathways and pathological features underlying the initiation and progression of AD and PD; although

many hypotheses have been put forward, the only histopathological feature characterizing these diseases is still represented by amyloid inclusions. In particular, these entities are Lewy Bodies (LB) in PD, and intracellular neurofibrillary tangles (NFT) and extracellular amyloid plaques in AD [3,4]. These histopathological hallmarks strictly correlate with the amyloid hypothesis, which represents the most studied, but also the most controversial one. The association of this hypothesis with the aforementioned histopathological features underscores its prominence as one of the primary hypotheses of neurodegeneration [4].

Nowadays, AD diagnosis is based on a clinical evaluation and imaging investigation based on techniques such as positron emission tomography (PET), while a definitive diagnosis is confirmed only upon a post mortem examination of the patients' brain. The diagnosis requires the detection of dopaminergic neuron loss, together with the presence of LB and Lewy neurites for PD. NFT and amyloid plaques are instead required to validate the diagnosis of AD [5]. The diagnostic criteria and methods for other neurodegenerative diseases are even less reliable. CT (Computer Tomography) and MRI (Magnetic Resonance Imaging) scans of patients' brains are employed to provide information about the shape, position, or volume of the tissue, thus offering an overview of the progress of central nervous system (CNS) tissue deterioration when the disease is at an advanced stage. Several molecular imaging compounds have been studied so far, with four of them being approved for clinical use. In particular, Florbetaben, Florbetapir, and Flutemetamol have been approved for the detection of beta-amyloid plaques in the brain, and Flortaucipir F18 for the detection of Tau neurofibrillary tangles [6,7]. Even though amyloid plaques in the brain are a characteristic feature of AD, their detection through PET imaging cannot be used to diagnose the disease. Indeed, the presence of Tau neurofibrillary tangles correlates better with cognitive symptoms in AD with respect to that of amyloid plaques. Moreover, these latter aggregates are not easily detectable with A $\beta$  PET tracers. In addition, A $\beta$  aggregates cannot be considered as a specific hallmark of AD, as amyloid plaques are frequently also found in dementia with Lewy bodies (i.e., the second most common degenerative dementia), as well as in blood vessels in cerebral amyloid angiopathy. Therefore, patients with these conditions show high signals on amyloid PET scans that are similar in pattern to those seen in AD [8,9].

## 2. Strategies for the Diagnosis of Pre-Symptomatic Neurodegenerative Diseases

Significant advances have been made in amyloidosis imaging so far; however, methods that can help to diagnose and differentiate among patients with neurodegenerative disorders, ideally pre-symptomatically, are still missing. The identification of novel strategies for diagnosis at the incipient stages of Alzheimer's disease, i.e., before irreversible brain damage or mental decline has emerged, represents one of the most active research areas. Notably, research and clinical findings have highlighted features and biomarkers whose levels significantly change before the onset of early symptoms of these diseases. For example, amyloid beta peptides (A $\beta$ ), truncated Tau proteins, and phosphorylated forms of Tau (p-Tau) are few among the main pathological biomarkers whose detection has been progressively implemented, allowing for the detection of a prodromal form of the disease. Their quantification is commonly performed on cerebrospinal fluid (CSF), a medium collected through lumbar punctures. There are three main ELISA-based methods that have been approved as in vitro diagnostic kits for the quantification of A $\beta$  peptides: Innostest<sup>®</sup> ELISA, IBL International<sup>®</sup> ELISA, and Euroimmun<sup>®</sup> ELISA. Despite their good correlation with PET imaging, these methods still present pre-analytical issues, such as: (i) the absorption to the fluid collection tubes, generating false positive results; (ii) the pretreatment of CSF samples using denaturation in guanidine hydrochloride, and (iii) the time and volume of fluid collection not being fully standardized. In addition, even if immunoassay platforms making use of fluorescence, chemiluminescence, or electrochemiluminescence for detection are valuable approaches for quantification (due to their high sensitivity), they still have the disadvantages of inter- and intra-assay variability. This is mainly because of peptide detectability issues that can derive by the high propensity of

amyloids to bind to other proteins, often hiding the epitopes recognised by the antibodies. Another drawback of ELISA-based approaches is their intrinsic inability to fully identify pathological oligomers, which may also be undetectable due to their incorporation into larger aggregates. Indeed, antibodies often detect only specific conformations of aberrant proteins; thus, structurally different A $\beta$  species in the sample remain undetected [8,10].  $\alpha$ -synuclein pathological species can be detected in CSF using real-time quaked induced-conversion (RT-QuIC) and protein-misfolding cyclic amplification (PMCA). Interestingly,  $\alpha$ Syn pathological aggregates detected by these methods are proven to discriminate between PD and other synucleinopathies such as multiple system atrophy (MSA), suggesting that different polymorphs and strains are present in these diseases [11,12]. In the last years, Tau aggregates have been observed in aberrant quantity within different fluids, the most studied being CSF [13–15]. Notably, Tau oligomers aberrantly accumulate in the early phases of tauopathies, and their concentration reflects neurodegeneration progression [13–15], particularly for AD [16,17]. While the concentration of biomarkers such as total Tau (t-Tau) and phosphorylated Tau (p-Tau) have been observed to increase early in tauopathies, the diagnosis and discrimination of these pathologies from CSF fluid biomarking present several challenges, such as the invasiveness of fluids collection and the variability across different cohorts of patients [13,16,18,19]. Another potential biofluid for the early detection of tauopathies is blood, whose analysis presents advantages in terms of the personnel and facilities required, being less invasive than CSF collection [20–22]. Unfortunately, there are also several issues related to the identification of Tau biomarkers in blood, like the significantly lower concentration of Tau species in this medium compared to CSF [15]. The introduction of ultrasensitive single molecule array (Simoa) technology and mesoscale discovery (MSD) ELISA methods recently enabled the identification of blood Tau biomarkers in large populations of patients [23–25], demonstrating that p-Tau may help to discriminate AD from other tauopathies [11,23,24,26–28]. However, it should be pointed out that most research related to the identification of Tau biomarkers in blood has been focused on AD [23,26–29]. Therefore, further efforts are needed to fully understand the utility of blood Tau biomarkers for the early diagnosis and characterization of other tauopathies [30]. Together with blood, urine has also become one of the most studied fluids for Tau biomarkers' detection [31,32]. For example, it has been recently demonstrated that t-Tau can be detected in urine samples from patients with acute neuronal and glial damage [33]. Considering the low invasiveness and applicability of urine tests in routine controls, future efforts should be addressed towards the identification of biomarkers facilitating the monitoring of the development and progression of tauopathies. Additionally, saliva could also potentially be investigated for pathological Tau detection [34–39]. For example, altered p-Tau/T-Tau ratios have been observed in saliva samples from patients with AD, with respect to the control population in a recent study [34]. Similar results were observed by Marksteiner and co-workers [35], who found significantly higher levels of p-Tau181 and lower t-Tau levels in salivary samples from AD patients [35]. On the contrary, similar t-Tau concentrations were observed in saliva from patients with AD, MCI, or healthy controls in a recent study by Ashton et al. [40]. These different outcomes may be explained by saliva composition heterogeneity, as well as restricted patient cohort analysis [41]. Interestingly, multiple immunoassay platforms and cross-sectional studies have found that t-Tau and p-Tau levels vary in the tears of patients affected by neurodegeneration, with respect to healthy controls [42–44]. As for saliva, further research in larger cohorts of patients is needed to confirm the predictive value of Tau biomarking in tears for the diagnosis of AD and other tauopathies. Finally, nasal secretions are currently under investigation for the possible detection of tauopathies biomarkers [45–47]. Statistically different p-Tau/t-Tau ratios in AD patients were found with respect to the control population in Arrozi's study, but further research in larger cohorts of patients is needed to confirm the validity of this biofluid for tauopathies monitoring [48]. To date, the detection of Tau aggregates and tauopathies biomarkers in biofluids has gained interest, especially for cost-effective and non-invasive

mediums. However, larger patient cohorts are needed, and variability problems still have to be addressed for the efficient early diagnosis of Tau-related diseases.

The use of fluorescent probes represents a valuable methodology for monitoring, in real time, the full-time course of aberrant protein aggregation, from monomeric peptide or protein to amyloid, having single-particle sensitivity. However, the expensiveness of the facilities needed for the analyses and the risk of radiation exposure for the current modalities of molecular imaging applied in clinical studies represent inevitable limitations. Therefore, Near-Infrared (NIR) fluorescent imaging (NIRF) has recently attracted attention as a promising non-invasive method for visualizing amyloid plaques *in vivo* (eye scan technology) or in biofluids (CSF, urine, and saliva) (Figure 1) [8]. Compared to PET and single-photon emission computed tomography (SPECT), NIRF has many advantages, such as safe and sensitive detection without radiation damage, moderate cost, and minimal auto fluorescence of the NIR probes from cellular and tissue components. Fluorescent amyloid-binding agents offer substantial opportunities for basic research on amyloid composition. Several efforts have been made in the field of bioimaging using non-invasive NIR probes in the frame of neurodegenerative diseases, particularly for AD diagnosis. Despite their favorable features for *in vivo* application, their translation into preclinical and clinical practices remains challenging, and further optical improvements and technological evolutions are still needed. In particular, there is a need for new NIR fluorescent probes based on new scaffolds, which are able not only to be selective for distinct amyloid aggregates (e.g., A $\beta$ , Tau, hIAPP, or  $\alpha$ -synuclein), but also to be selective over soluble species, such as oligomers. The exploration of new probes that selectively target oligomers of one type of amyloid protein is a priority for future research, because oligomers are produced before the accumulation of plaques and thus can be exploited as early biomarkers of the pathological process, long before symptoms have appeared. When new NIR fluorescent probes that are selective for oligomers and able to distinguish different amyloid aggregates are available, it will be possible to translate NIRF imaging into future clinical applications (Figure 1).

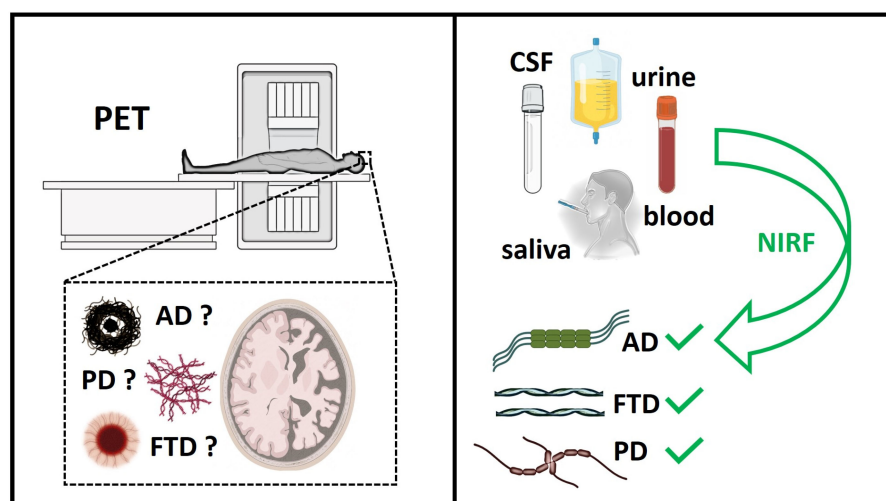


**Figure 1.** Schematic representation of two different diagnostic approaches in neurodegeneration through PET (Positron Emission Tomography) and Near-Infrared (NIR) fluorescent imaging (NIRF), discussed in this review.

In this review, we aim to provide a general overview of the main achievements in the development of fluorescent probes for the detection of amyloid aggregates in the frame of AD and PD. Since a significant number of reports have already been published for the A $\beta$ <sub>1–42</sub> peptide [49–51], this review will firstly show the main advantages and disadvantages of the approaches currently reported for the design of fluorescent probes detecting A $\beta$ <sub>1–42</sub> toxic oligomers. Afterwards, a discussion in the same regard will be dedicated to the Tau protein, whose detection is still under research investigation, especially for the

validation of biomarkers' outcomes. Finally, a section will be dedicated to  $\alpha$ -synuclein, to give the opportunity to the readers interested in fluorescent chemical tools to realize what has been achieved in PD diagnosis to date, and to compare it to that made in AD diagnosis, thus giving the opportunity to take inspiration for future applications in diagnosis. In particular, we focused on three main goals, i.e., (i) to compare and find similarities/differences between the probes developed for  $\alpha$ Syn and those concerning Tau and  $A\beta_{1-42}$ ; (ii) to give insights on the use in ex vivo and in vivo systems of these compounds for future diagnosis application; and (iii) to discuss on the main achievements on the detection of amyloids in biofluids. By critically dissecting the strengths and weaknesses of the main probes provided in the literature, we believe this will help the research on neuropathology to advance into neurodegeneration prevention and future early diagnosis without the need for hazardous and costly approaches.

### 3. Approaches in $A\beta_{1-42}$ , Tau and $\alpha$ Syn Probing

#### 3.1. $A\beta_{1-42}$ Peptide Probes

To date, chemically different NIR probes have been designed and evaluated for binding to various  $A\beta$  peptides, especially the insoluble fibers of amyloid plaques (Table 1). Fluorescent probes derivatized from styryl scaffold (Figure 2A) have been proposed [9,52–55], but even if they were able to cross the blood–brain barrier (BBB), they could not be employed for in vivo imaging because of their low affinity for  $A\beta$  plaques and their excitation and emission still outside of the NIR region. Oxazine dyes (Figure 2B) have allowed for improving the fluorescence properties of NIR probes by increasing the quantum yield (41%) upon binding to  $A\beta$ s and the wavelengths of absorption/emission (650–670 nm) [56].

**Table 1.** In the table, the probes selectively recognizing one specific kind of amyloid aggregate are reported. The selectivity towards a specific amyloid species ( $\alpha$ Syn,  $A\beta_{1-42}$ , Tau) is also indicated, as well as the mechanism by which the probe interacts with its target.

Compounds	Aggregate Selectivity	Amyloid Selectivity	Mechanism of Interaction
Styryl derivatives	None ( $A\beta_{1-42}$ aggregates)	$A\beta_{1-42}$	Possible intercalation in $\beta$ -sheet-rich structures
Oxazine dyes	None ( $A\beta_{1-42}$ aggregates)	$A\beta_{1-42}$	Possible intercalation in $\beta$ -sheet-rich structures
2,2'-bithiophene derivatives	None ( $A\beta_{1-42}$ fibrils, amyloid aggregates)	None	Binding to amyloid fibrils surface
Curcumin derivatives	Oligomers and fibrils	None ( $\alpha$ Syn, $A\beta_{1-42}$ , Tau)	Not specified
Chalcone derivatives	$A\beta_{1-42}$ plaques	$A\beta_{1-42}$	Not specified
1,4-naphthoquinones	None ( $A\beta_{1-42}$ aggregates and plaques)	$A\beta_{1-42}$	Not specified
BODIPY dyes	Oligomers and fibrils	$A\beta_{1-42}$	Binding to hydrophobic surfaces
CRANAD-3	None (different oligomers, monomers)	$A\beta_{1-42}$	Not specified
BD-Oligo probe	Oligomers	$A\beta_{1-42}$	Similar to BODIPY dyes
BODIPY-6 and aza-BODIPY	Oligomers and fibrils	$A\beta_{1-42}$	Similar to BODIPY dyes
PTO-29	Oligomers	$A\beta_{1-42}$	Not specified
F-SLOH	Oligomers	$A\beta_{1-42}$	Not specified
$[^{18}\text{F}]$ -FDDNP	None (Tau aggregates)	$A\beta_{1-42}$ , Tau	Not specified
$[^{11}\text{C}]$ -PBB3	None (Tau aggregates)	$A\beta_{1-42}$ , Tau	Not specified
THK compounds ( $[^{18}\text{F}]$ -THK-523, $[^{18}\text{F}]$ -THK-5105, $[^{18}\text{F}]$ -THK-5116, $[^{18}\text{F}]$ -THK-5117 and $[^{18}\text{F}]$ -THK5351)	None (Tau aggregates)	Tau	Not specified
Flortaucipir (18F)	Tau fibrils (PHF)	Tau	Not specified
$[^{18}\text{F}]$ -GTP1	Neurofibrillary tangles (NFT)	Tau	Not specified
$[^{18}\text{F}]$ -JNJ069	Neurofibrillary tangles (NFT)	Tau	Not specified
$[^{18}\text{F}]$ -JNJ311	Neurofibrillary tangles (NFT)	Tau	Not specified
$[^{18}\text{F}]$ / $[^3\text{H}]$ -MK-6240	Neurofibrillary tangles (NFT)	Tau	Not specified



Table 1. Cont.

Compounds	Aggregate Selectivity	Amyloid Selectivity	Mechanism of Interaction
[ <sup>18</sup> F]/[ <sup>3</sup> H]-PI-2620	Neurofibrillary tangles (NFT)	Tau	Not specified
[ <sup>18</sup> F]/[ <sup>3</sup> H]-RO-948	Neurofibrillary tangles (NFT)	Tau	Not specified
Shiga-X34	Tau NFT	Tau	Not specified
Shiga-X35	None (Tau NFT and other aggregates)	Tau	Not specified
Quinoline-based probes (Q-tau1 and Q-tau4)	None (Tau aggregates)	Tau	Not specified
pTP-TFE	None (Tau soluble aggregates)	Tau	Not specified
BODIPY-derived probes (BT1)	Tau oligomers (phosphorylated)	Tau	Similar to BODIPY dyes
Anle138b	Oligomers and fibrils	None ( $\alpha$ Syn, A $\beta$ <sub>1–42</sub> , Tau)	Possible methyl bridge disruption leading to free hydroxyl (H-bond interaction), intercalation in $\beta$ -sheet-rich structures
PP-BTA-4	Fibrils	$\alpha$ Syn, A $\beta$ <sub>1–42</sub>	Not specified
[ <sup>11</sup> C]SIL5	Fibrils	$\alpha$ Syn	Not specified
[ <sup>125</sup> I]SIL23	Fibrils	$\alpha$ Syn	Not specified
[ <sup>18</sup> F]SIL26	Fibrils	$\alpha$ Syn	Not specified
[ <sup>18</sup> F]46a	Fibrils	$\alpha$ Syn	Not specified
[ <sup>125</sup> I] IDP-3	None ( $\alpha$ Syn aggregates in LBs)	$\alpha$ Syn	Not specified
[ <sup>125</sup> I] IDP-4	None ( $\alpha$ Syn aggregates in LBs)	$\alpha$ Syn	Not specified
[ <sup>18</sup> F] 2FBox	None	$\alpha$ Syn and A $\beta$ <sub>1–42</sub>	Not specified
[ <sup>18</sup> F] 4FBox	None	$\alpha$ Syn and A $\beta$ <sub>1–42</sub>	Not specified
Anle253b	Fibrils	$\alpha$ Syn	Not specified, probably similar to Anle138b
(d3)-[ <sup>11</sup> C]MODAG-001	Fibrils	$\alpha$ Syn	Not specified
BQ-1	None	$\alpha$ Syn	Not specified
[ <sup>18</sup> F]BQ-2	None	$\alpha$ Syn	Not specified

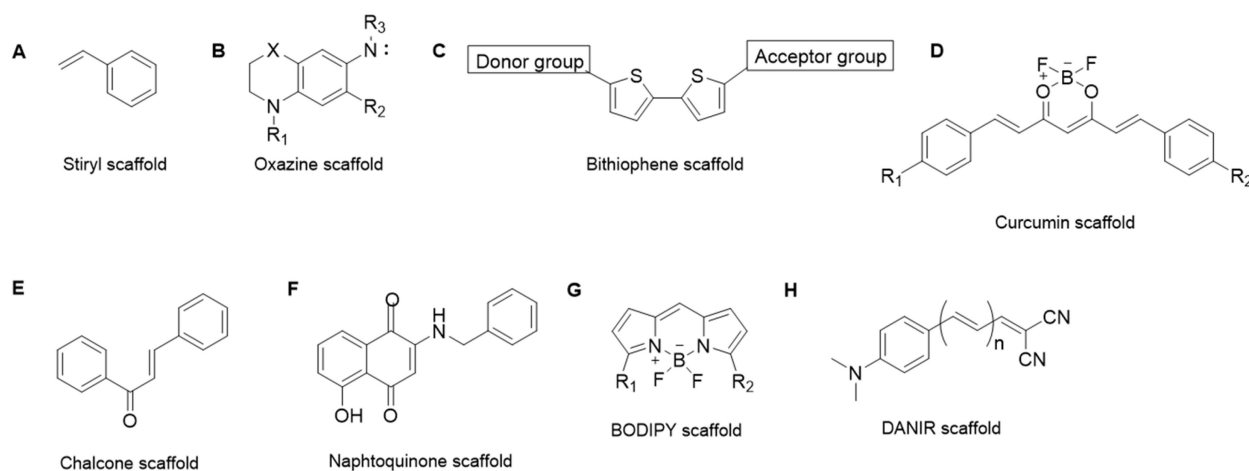


**Figure 2.** Representation of the different molecular scaffolds employed for the design of NIR probes detecting A $\beta$  aggregates: (A) (Styryl scaffold), (B) (Oxazine scaffold), (C) (Bithiophene scaffold), (D) (Curcumin scaffold), (E) (Chalcone scaffold), (F) (Naphthoquinone scaffold), (G) (Bodipy scaffold), (H) (DANIR scaffold).

However, the affinity for A $\beta$  plaques remains moderate and the detection sensitivity is still low because of their small Stokes shift. A series of 2,2'-bithiophene compounds (Figure 2C) possessing the classical push–pull architecture (electron–donor and electron–acceptor groups as terminal moieties, interconnected by a highly polarizable bridge) were reported in the early exploration stage and showed relatively simple structures and excellent fluorescent features, such as a high QY and high emission wavelength (720 nm max) [57,58]. The small planar structure, matching the features of amyloid fibrils surfaces, is responsible of their high binding selectivity to aggregate amyloids, but, at the same time, it is responsible for a lack of specificity for amyloid deposits and high-affinity binding with plasmatic proteins. Inspired by the natural compounds having high binding for

plaques, such as curcumin, researchers developed novel NIRF probes with good optical properties: fluorescence intensity increasing upon binding, blue shift, and a large increase in QY (Figure 2D) [59–61]. Despite their high affinity for A $\beta$  aggregates and high metabolic stability, these new probes exhibited a low selectivity between A $\beta$  subspecies, making them unsuitable for monitoring A $\beta$  oligomers at a presymptomatic stage of AD. New natural scaffolds for A $\beta$  imaging agents have been exploited after the observation of their direct interaction with A $\beta$  aggregates. Chalcone derivatives (Figure 2E) have been reported as PET/SPECT probes for in vivo imaging and proved to specifically stain the A $\beta$  plaques in brain sections from a transgenic AD model mouse. Starting from these results, a series of chalcone derivatives were developed as NIRF probes with improved characteristics, such as plaque affinity and fluorescent properties [62,63]. Despite this, their low micromolar affinity and short excitation/emission wavelength (400 nm/532 nm) prevent their application. Recently, 1,4-naphthoquinones (Figure 2F) have been presented as a novel scaffold for the future designs of drugs and new diagnostic tools that can target both dense-core and diffuse plaques (amorphous deposits that lack dense cores or dystrophic neuritis) [64]. Boron dipyrromethene (BODIPY, Figure 2G) is one of the most widely used small-molecule organic fluorophores in bioimaging. In the literature, several probes based on BODIPY have been proposed for A $\beta$  imaging, but most of them have not yet been reported to image A $\beta$  in vivo due to a high background signal (nonspecific binding) and the difficulty in obtaining a good balance between the polarity of compounds and desirable emission properties [65–68]. Recent efforts toward the development of new BODIPY-based probes have led to a new PIET (photoinduced electron transfer) quenched NIR probe, containing BODIPY as a fluorophore and tetrahydroquinoxaline as a quenching group. This molecule was found to be able to detect both fibrils and oligomers with significant fluorescent switch-on after binding to soluble and insoluble A $\beta$  species. This new quenching strategy allowed for reducing the intrinsic fluorescence of the probe and thus increasing its QY (quantum yield) upon binding [69].

Finally, the donor–acceptor architecture bridged by a conjugated  $\pi$ -electron chain (push–pull architecture) is still now the method of choice for the design of donor–acceptor NIR probes (DANIR, Figure 2H). The strategy for creating larger conjugated systems is based on the hypothesis that this type of molecules could have more potential to bind to A $\beta$  aggregates and plaques. At the same time, this approach has a bad impact on the QY of the probe, because the unbound probe is already highly fluorescent. Therefore, the research in this field is still working on finding a correct balance between the  $\pi$ -conjugation system and the properties of probes [70–73]. If the exploitation of diagnostic probes for A $\beta$  fibers and plaques has encountered great research interest in recent years, this is not the case for NIR probes for oligomers binding. A first example is a curcumin-based NIRF imaging probe, which resulted in being unsuitable for in vivo imaging due to its short excitation and emission wavelengths [59]. Different modifications were designed to have a longer  $\pi$ -conjugation system while preserving the binding affinity [74,75]. Until now, CRANAD-3 (curcumin scaffold in Figure 2D) is the probe that exhibited the strongest affinity with A $\beta$  monomers, dimers, and oligomers [76]. However, these curcumin analogs possess a low QY and low selectivity between A $\beta$  subspecies. Specificity was almost achieved after several optimizations of the BODIPY scaffold, which led to the discovery of the BD-Oligo probe. This probe has a high fluorescence enhancement upon incubation with A $\beta$  oligomers, which decreases as more A $\beta$  assembles into fibrils. However, despite its oligomer-sensing ability, this probe suffers from a low binding affinity and short wavelength excitation [77].

The triazole-containing BODIPY-6 and aza-BODIPY are fluorescent dyes showing interactions with soluble and insoluble amyloid aggregates. They have been employed for the co-staining of A $\beta$  in brain tissues and proved to be able to induce a contrasting signal, which can help to monitor the conformational transition of fibrils and oligomers [68,78]. A novel “V-shaped” NIR A $\beta$  oligomer-specific fluorescent probe, PTO-29 [79], demonstrated good photophysical properties and selective recognition of A $\beta$  oligomers over other A $\beta$ s in a solution test and phantom imaging study. PTO-29 also showed good BBB penetration

and a low cytotoxicity, and it was successfully employed to image 4-month APP/PS1 mice *in vivo*. The *in vitro* fluorescence staining of A $\beta$  oligomers on age-matched Tg mouse APP/PS1 has been also performed with a probe characterized by two electron-donating N,N-diethylaniline recognition groups bonded to a single-boron difluoride bridge azafluorene as the strong electron-withdrawing group [80]. Finally, a novel fluoro-substituted cyanine probe, F-SLOH, demonstrated a good A $\beta$  oligomer selectivity with a high binding affinity. The selectivity towards the A $\beta$  oligomers in the brain was ascertained by *in vitro* labelling on tissue sections and *in vivo* labelling through the systemic administration of F-SLOH in 7-month APP/PS1 double-Tg and APP/PS1/Tau triple-Tg mouse models [81]. However, to our knowledge, all the listed fluorescent probes have not been studied for their specificity for amyloids associated with specific diseases. Due to their significant aromatic character, it is likely that these types of molecules are not able to discriminate between different amyloid proteins, thus preventing their employment as clinical tools for establishing the early and accurate diagnosis of neurodegeneration in different, but closely related, diseases.

### 3.2. Tau Probes

Tau is a highly conserved and soluble protein, classified among the so-called “Intrinsically Disordered Proteins” [82]. Six different Tau isoforms of 352–441 amino acids are currently known, which differ for the presence of zero (i.e., 0 N), one (i.e., 1 N), or two (i.e., 2 N) amino acid (AA) sequence inserts at the N terminal side of the protein, and by three or four AA small-sequence repeats at the C-terminus (commonly known as 3R and 4R, respectively); each isoform derives by the alternative splicing of the MAPT (microtubule-associated protein tau) gene [83,84]. Tau is mainly present in neuronal cells, where it is involved in the regulation of the stability of axonal microtubules and in the control of several other cellular signaling processes [85]. Upon a series of genetic and post-translational modifications (PTMs), Tau can present a reduced affinity for microtubules, resulting in their destabilization [85–88]. Moreover, when detached by microtubules, Tau can aberrantly accumulate into the cell cytoplasm, aggregating into toxic multimeric complexes responsible for neuronal cell death [89,90]. Indeed, several clinical and research findings have shown in recent years that aberrant aggregates of Tau participate in the development and progression of a number of neurodegenerative disorders and dementias, collectively named as tauopathies [54,91]. As a consequence, Tau has become a relevant therapeutic target for the development of agents disrupting aberrant aggregates or preventing their formation. However, no drugs have been approved to date for the treatment of tauopathies. Furthermore, Tau PTMs have emerged as potential biomarkers for the early identification and diagnosis of tauopathies, and research endeavors have also been conducted towards their identification in human biofluids, especially by the means of non-invasive techniques [14,92–98]. Imaging and detection in Tau aggregates is of primary importance, and significant research has also been devoted towards the identification of probes that facilitate the monitoring of different tauopathies; the diagnosis of such diseases is still based on imaging techniques and clinical evaluation is often confirmed only after an examination of patients’ brains [99–102]. Several methods are currently available to help in this respect, with positron emission tomography being one of the most employed for neuroimaging deposits of Tau. Indeed, PET presents several advantages for the diagnostic imaging of Tau, including its relatively low invasiveness and a number of already reported molecular probes targeting this protein with a good specificity and affinity, also *in vivo* [103,104]. Such probes can help to detect abnormal Tau aggregates accumulating in different districts of the human brain, already at the early phases of neurodegeneration. Hence, they represent valuable complementary tools for monitoring tauopathies’ progression [103]. Moreover, PET imaging might help to differentiate between tauopathies based on different Tau isoforms (e.g., 3R, 4R, and 3R + 4R), through the use of specific tracers [105]. A number of PET probes are currently available for detecting Tau deposits in preclinical and clinical settings (Figure 3 and Table 1). One of the first reported Tau tracers



is [ $^{18}\text{F}$ ]-FDDNP, which has demonstrated valuable performances in AD monitoring, albeit showing a poor ability to differentiate aggregates of Tau from A $\beta$ -related ones [106]. In addition, [ $^{11}\text{C}$ ]-PBB3 [107] has demonstrated being able to differentiate AD patients from healthy controls, and is able to detect Tau aggregates in subjects with dementias not related to Alzheimer's disease; however, this compound poorly discriminated among Tau/A $\beta$  deposits [108]. Tau tracers based on a quinoline scaffold, which are also known as "THK compounds", have also been reported [109–116], demonstrating a significant selectivity for Tau aggregates with respect to A $\beta$ -related ones. Among the first of this class are [ $^{18}\text{F}$ ]-THK-523, [ $^{18}\text{F}$ ]-THK-5105, [ $^{18}\text{F}$ ]-THK-5116, and [ $^{18}\text{F}$ ]-THK-5117. [ $^{18}\text{F}$ ]-THK-523 has also displayed low accumulation in patients' brains, while [ $^{18}\text{F}$ ]-THK-5105 and [ $^{18}\text{F}$ ]-THK-5117 showed uptakes well correlated with Tau-related disease progression [109–115].

Later, [ $^{18}\text{F}$ ]-THK5351 demonstrated improved PET imaging performances [116]. However, it also showed issues related to poor absorption in patients' brains, concurrently with the administration of monoamine oxidases (MAOs) inhibitors; this is an issue that has been highlighted for several probes reported for Tau PET imaging [116]. Additionally, compounds based on the 5,9b-dihydro-4aH-pyrid[4,3-b]indole scaffold have also been investigated, with Flortaucipir (18F) (i.e., [ $^{18}\text{F}$ ]-AV-1451, [ $^{18}\text{F}$ ]-T807) being the only radiotracer approved for imaging Tau deposits in vivo [117,118]. This molecule demonstrated being promising in clinical settings and showed no contraindications for Tau PET imaging; scenarios in which Flortaucipir (18F) can be used for diagnosis and monitoring have also been suggested [118,119], as well as its limitations in detecting early-stage Tau pathology [120]. Notably, Flortaucipir (18F) has shown a good BBB permeability and high affinity for Tau paired helical filament (PHF) aggregates in patients with Alzheimer's disease [121]. However, 18F-flortaucipir can accumulate into pigment-containing and calcified structures in the brain, and it can also bind to monoamine oxidases, thus potentially affecting its specificity in imaging analyses [122–124].

Overall, several among the first reported PET probes of Tau present limitations, including, for example, a low selectivity for Tau versus A $\beta$  aggregates in some cases, and a low specificity for white matter in the brain, thus altering imaging contrast [103,119,125]. Moreover, several of these probes were not able to discriminate between different Tau deposits. These limitations fueled the development of novel Tau PET tracers such as [ $^{18}\text{F}$ ]-GTP1, [ $^{18}\text{F}$ ]-JNJ069, [ $^{18}\text{F}$ ]-JNJ311, [ $^{18}\text{F}$ ]/[ $^3\text{H}$ ]-MK-6240, [ $^{18}\text{F}$ ]/[ $^3\text{H}$ ]-PI-2620, [ $^{18}\text{F}$ ]/[ $^3\text{H}$ ]-RO-948 (i.e., [ $^{18}\text{F}$ ]/[ $^3\text{H}$ ]-RO6958948), [ $^{18}\text{F}$ ]-APN-1607 (i.e., [ $^{18}\text{F}$ ]-PM-PBB3), [ $^{11}\text{C}$ ]-RO6931643, [ $^{11}\text{C}$ ]-RO6924963, and [ $^{18}\text{F}$ ]-SNFT-1 [126–130] (Figure 3), with these compounds showing significantly less off-target binding to aggregates and better pharmacokinetic properties. Moreover, several of these compounds showed improved pharmacokinetic properties and the ability to discriminate AD from non-AD tauopathies. Examples in this regard are the compounds [ $^{18}\text{F}$ ]-MK-6240, [ $^{18}\text{F}$ ]-PI-2620, [ $^{18}\text{F}$ ]-RO-948, and [ $^{18}\text{F}$ ]-APN-1607, which showed good performances in discriminating AD from non-AD patients in in vivo PET imaging studies [131–134], and also helping to detect low levels of Tau. Altogether, these data can offer insights into the design of compounds targeting Tau aggregates [135–138]. The utility of Tau PET tracers for the early diagnosis and monitoring of AD has also been studied in combination with assessments of phosphorylated Tau, providing remarkable results [139]. However, further research is needed to better assess their utility in clinical settings [103,119,131]. In particular, most of the studies reported so far focused on AD and related dementias, and, to a lesser extent, CBD (Corticobasal Degeneration), CTE (Chronic Traumatic Encephalopathy), FTL (Frontotemporal Lobar Degeneration), PiD (Pick's Disease), and PSP (Progressive Supranuclear Palsy). In this respect, future research focusing on additional tauopathies is expected to provide fruitful insights into a better understanding of Tau-related diseases. While PET tracing is an established method for neurodegenerative diagnosis, imaging pathological Tau might also present some intrinsic limitations. For example, results of in vivo Tau PET imaging performed in post mortem brains of AD patients often resulted in not being fully in agreement with disease progression [125]. In addition, the high costs and exposure risks associated with the use of radioligands cannot

be neglected, as this could hamper routine monitoring. It is worth noting that studies on the use of benzimidazole compounds such as lansoprazole and astemizole (Figure 3) as potential PET tracers have also been conducted [140,141], demonstrating that they might have great potential in radio-labelled neuroimaging for the *in vivo* early detection of AD. To date, no successful stories focusing on the repositioning of already approved drugs towards Tau PET imaging have been reported. However, these aspects are of particular interest and could suggest novel sources and approaches for rapidly identifying PET tracers for tauopathies investigations. Besides PET, magnetic resonance imaging has also been used to provide insights into AD and tauopathies in different settings [141,142]. Indeed, MRI presents several advantages with respect to PET for Tau imaging. For example, it does not employ ionizing radiation in its assessments. While such techniques show large possibilities of application for studying changes in the brains of patients, approaches and probes based on MRI potentially useful for the molecular imaging of Tau are still under development [141–145]. Indeed, only few studies have reported the use of MRI-based Tau imaging with contrast agents, the majority of them being focused on animal models and employing fluorinated compounds [142]. One among the first studies reporting the use of a fluorine-19-labeling compound (i.e., Shiga-X34, Figure 3), by the means of fluorine-19 magnetic resonance imaging (19F-MRI) [146,147], was reported by Yanagisawa et al. in 2018 [148]. In that study, the authors performed *ex vivo* analyses on rTg4510 mice, demonstrating that their compound Shiga-X34 can bind to NFTs of different tauopathies. In this study, Shiga-X34 was also used as a starting point for the development of a 19F-MRI additional probe for Tau imaging (i.e., Shiga-X35). Notably, Shiga-X35 (Figure 3) showed efficient detection abilities for Tau NFTs, as observed by the means of 19F-MRI imaging in rTg4510 mice, and readily reached the brain after injection, although was gradually excreted with some undesirable accumulation [148]. However, Shiga-X35 presents a low specificity and selectivity for NFTs and senile plaques, suggesting that further optimization on this scaffold is required. Besides Shiga-X35, an additional MRI probe (i.e., the DNA-aptamer nanoparticle TauX) was reported by Badachhape et al. [149]. Notably, this product demonstrated enhancing the MRI signal in the transgenic PS19 mice line, 4 to 6 months before the subjects showed tauopathy symptoms. As a further note, studies employing artificial intelligence (AI) techniques to analyze MRI-image-related data and other readily available information for predicting the clinical status of patients with neurodegenerative diseases have very recently been proposed and applied for amyloids [150–153]. An example of this comes from a very recent study by Lew and colleagues [154], who reported the development and application of a deep learning approach able to predict the PET-determined amyloid-tau-neurodegeneration (ATN) biomarker status from MRI and other patient-related data reported in the Alzheimer’s Disease Neuroimaging Initiative (ADNI) database ([www.adni-info.org](http://www.adni-info.org), accessed on 29 November 2023). Notably, the study demonstrated good prediction performances and the agreement of the developed AI models with respect to the PET outcomes for ATN biomarking status. While the study presents some limitations, the results suggest that future advances in MRI techniques and their integration with AI approaches might provide diagnostic performances comparable to PET imaging, with reduced costs, time, and risks.

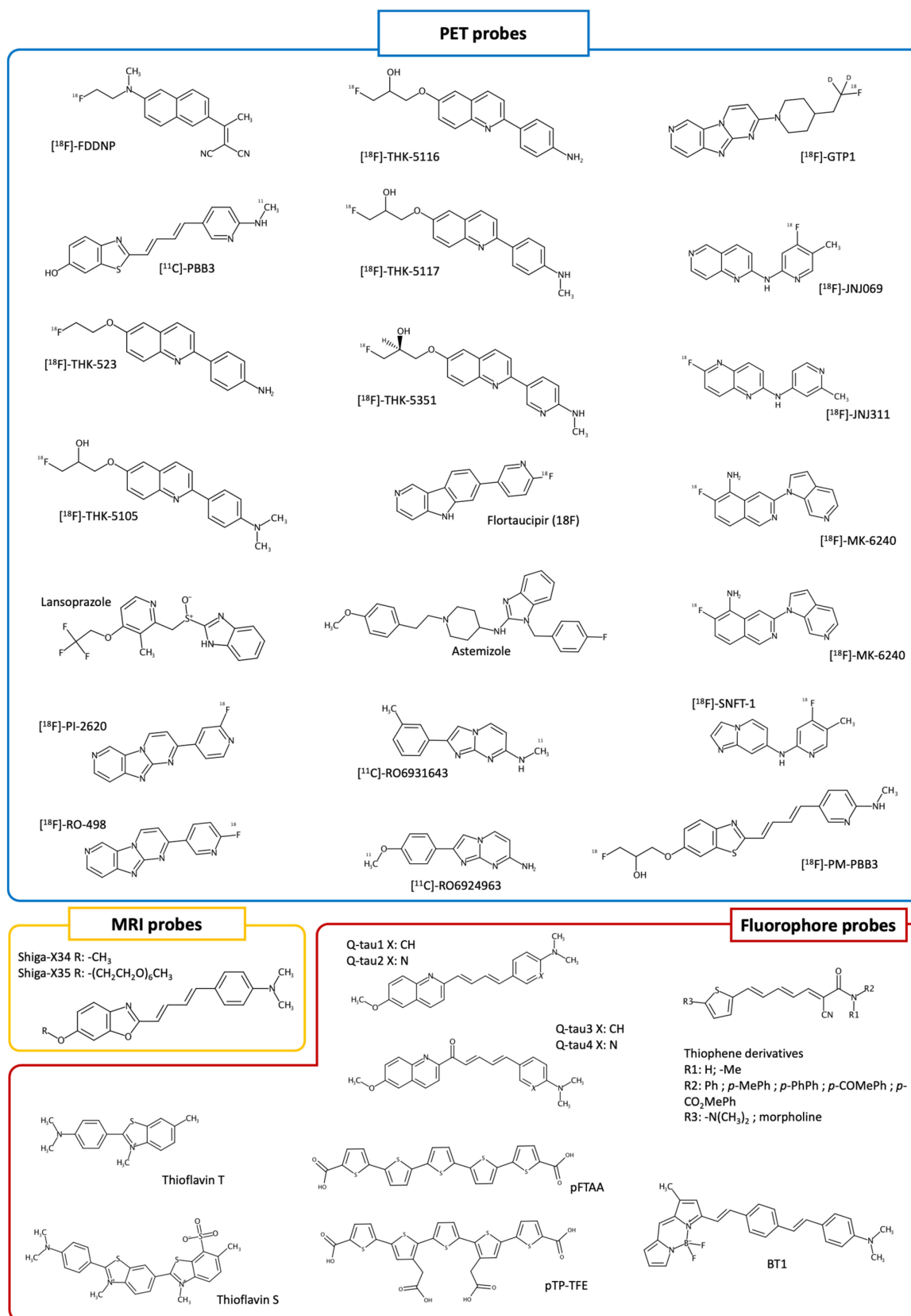


**Figure 3.** Chemical structure of PET, MRI, and fluorophore probes detecting Tau, discussed in the review.

To the best of our knowledge, there are no PET or MRI probes for selectively imaging Tau soluble aggregated species as oligomers, though these are considered to be among the most toxic components in tauopathies. In this context, fluorescent-probing techniques might provide several advantages, such as improved cost effectiveness and a high sensitivity and specificity. Indeed, in the last years, fluorescent probes such as thioflavin T (ThT) or thioflavin S (ThS) (Figure 3), whose fluorescence increases upon binding to Tau aggregates, have been introduced in experimental assays assisting the design of preclinical candidates [155,156]. However, their applicability is restricted only to *in vitro* experiments, and they very often require complementary experimental confirmations due to their low binding specificity towards different aggregates. Imaging Tau aggregates *in vivo* can be challenging due to their structural similarity to the structure of A $\beta$  fibrils; however, fluorescent probes that specifically detect Tau aberrant deposits have been very recently studied [157–160]. Among them, we can find the quinoline-based fluorescent probes (i.e., Q-tau 1 to 4, Figure 3) reported by Elbatrawy et al. [157], which showed a high selectivity towards Tau aggregates in *ex vivo* samples from AD brain tissues. Indeed, compounds Q-tau1 and Q-tau4 showed significant binding affinities toward Tau deposits, with selectivity indices of 4.4 and 3.5 over A $\beta$  aggregates, respectively. Moreover, Q-tau4 also showed: (i) a fluorescence signal that positively correlated with the immunofluorescence of p-tau; (ii) low cytotoxicity; and (iii) a selective fluorescent profile different from that of A $\beta$  plaques in AD brain tissues. Furthermore, in 2020, Zhao and co-workers reported compound pTP-TFE (Figure 3) that selectively binds to soluble Tau aggregates over mature fibrils [161]. Of note, this compound was developed starting from the p-FTAA probe (Figure 3) reported in 2009 by Åslund and colleagues [162], which showed a good BBB permeability and different spectral signatures when bound to A $\beta$  or Tau deposits; pTP-TFE was also demonstrated to be cell permeable. As a consequence, this compound represents a promising proof of concept tool for the study of tauopathies' development and progression [161]. Later, in 2021, Oh et al. [163] developed two additional series of thiophene derivatives (Figure 3) showing an improved selectivity for Tau aggregates, also in *in vitro* experiments on SH-SY5Y cells stably expressing GFP-tagged Tau. More recently, in 2022, Soloperto et al. [164] reported a focused library of eight BODIPY-derived probes, i.e., from BT1 to BT8, inspired by the selective fluorescent probe TAU1. These compounds feature conjugated systems of 13–19 Å length, ending with an electron donor group and characterized by a different polarity. Of note, one of them (i.e., BT1, Figure 3) showed favorable photophysical properties and a high selectivity towards phosphorylated and oligomeric Tau in an *in vitro* humanized cellular model; the results reported in this study paved the way towards the optimization of compounds potentially aiding in the early diagnosis of neurodegenerative diseases.

While the development of fluorescent imaging Tau probes is of primary interest, this field of research is still unfortunately in its infancy. Indeed, most of the fluorescent probes discussed above have been reported only very recently and studied in *in vitro* assays or *ex vivo* samples. Therefore, their potential translation into clinical use has yet to be proven. However, considering their potential for the diagnosis and monitoring of tauopathies, future research on fluorescent-based probes of Tau is warranted.

### 3.3. $\alpha$ -Synuclein Probes

#### 3.3.1. Florescent Probes

In the following paragraph, the current development of fluorescent probes for detecting  $\alpha$ Syn aggregation in *ex vivo* and *in vivo* systems is presented. A description regarding their selectivity against a specific amyloid or aggregate type is provided in Table 1.

Anle138b is a pyrazolo bearing 1,3-benzodioxole as a substituent in position 3 and 3-Br-phenyl in position 5 (Figure 4). Studies from Fields et al. show that it inhibits the formation and aggregation of  $\alpha$ Syn oligomers, without impacting the protein expression and physiological function. Also, the authors demonstrated that it decreases oligomer accumulation, neuronal degeneration, and PD progression in mice [165]. Interestingly, the anti-aggregation activity of the compound can be correlated to its 1,3-benzodioxole

ring. In cells, the methylene bridge between the oxygens might be disrupted, thus leading to two free hydroxyl groups. Although this could be the basis for the interaction with  $\alpha$ Syn, experimental data are needed to prove it. Notably, other experiments showed that its efficacy in disrupting oligomeric aggregates was due to the ability of intercalating among the  $\beta$ -sheets structures, present in the core of these species [165]. Finally, its efficacy was also proven against Tau and amyloid  $\beta$  aggregates [166]. In addition to inhibiting  $\alpha$ Syn oligomerization, anle138b showed significant fluorescence enhancement at around 345 nm after binding to  $\alpha$ Syn oligomers and fibrils. Interestingly, anle138b was able to interact and bind  $\alpha$ Syn fibrils with a  $K_d$  value of  $190 \pm 120$  nM. When the binding with  $\alpha$ Syn fibrils took place, an anle138b fluorescence increase occurred around 335 nm and was correlated with the decrease in the red wing fluorescence at  $\lambda > 385$  nm [167,168]. Due to the promising anti-aggregation activity of the compound, as well as its ability to bind  $\alpha$ Syn aggregates and displaying a strong fluorescence shift upon binding, anle138b provided a new possibility for the early diagnosis of PD. In particular, anle138b was proposed as a probe for the in vivo detection of retinal  $\alpha$ Syn deposition in combination with confocal scanning laser ophthalmoscopy as a non-invasive technique to spot early  $\alpha$ Syn aggregation. However, some limitations have hampered its development as an  $\alpha$ Syn fluorescent probe in non-invasive in vivo detection. The main limits are the moderate affinity for  $\alpha$ Syn aggregates, together with the lack of affinity regarding amyloid species ( $\alpha$ Syn, Tau, and amyloid  $\beta$ ) and its spectral properties [168–170]. However, this study indicated that  $\alpha$ Syn aggregation inhibitors might be a way to exploit the development of imaging probes.

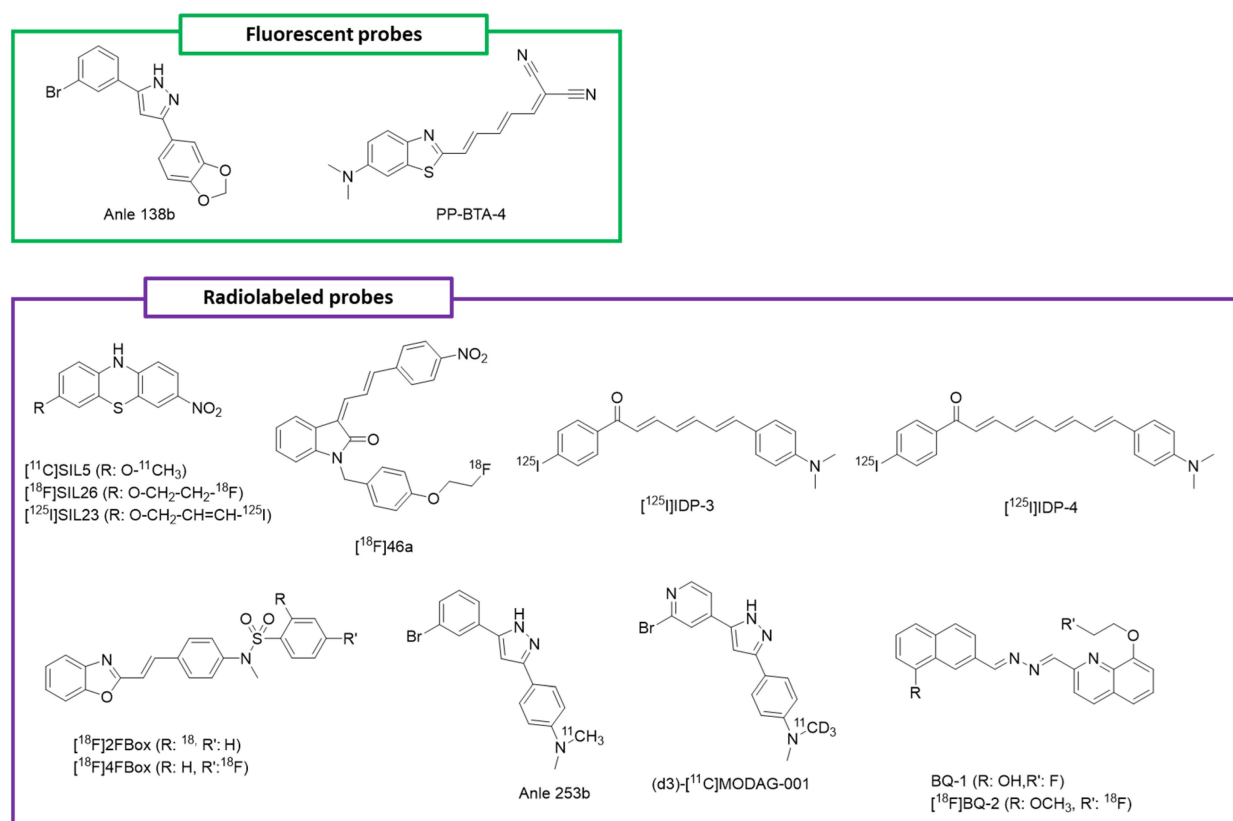


**Figure 4.** Probes for the detection of  $\alpha$ Syn aggregation discussed in the review.

Novel benzo-thiazole derivatives as potential fluorescent probes were developed by Watanabe et al. in 2017 [171]. Among them, PP-BTA-4 (Figure 4) presented an excitation/emission profile in chloroform of 559/727 nm. Upon binding with  $\alpha$ Syn aggregates, PP-BTA-4 presented a considerable fluorescent shift to 682/782 nm. Furthermore, this compound showed a high binding affinity for  $\alpha$ Syn aggregates in vitro with a  $K_d$  value



of  $48 \pm 0.6$  nM. As the background autofluorescence was low in the near-infrared region (650–900 nm), the emission wavelength of this compound was considered to be adequate for the detection of  $\alpha$ Syn aggregates in brain sections [171]. In human PD brain slices, where Lewy bodies were present, PP-BTA-4 stained some regions that were positive for immunohistochemical staining with a specific  $\alpha$ Syn antibody [171]. However, this compound lacked amyloid selectivity. In fact, it was able to recognize and bind to  $A\beta_{1-42}$  aggregates in vitro and in ex vivo samples (AD brain slices with  $A\beta_{1-42}$  plaques).

Although PP-BTA-4 had no selectivity for  $\alpha$ Syn and  $A\beta$  aggregates, it contributed to filling the gap of near-infrared (NIR) fluorescence probes to detect  $\alpha$ Syn fibrils. Through optimization and chemical modification, the compound may serve as an NIR fluorescent probe for the detection of  $\alpha$ Syn and  $A\beta_{1-42}$  aggregates in human brains [171].

These studies elucidate the lack of a specific, highly selective fluorescent probe for the detection of  $\alpha$ Syn inclusions in ex vivo and in vivo samples. The main limit characterizing the candidates developed up to now is the affinity for a determined  $\alpha$ Syn species (oligomers and fibrils), as well as amyloid specificity (selectivity towards  $\alpha$ Syn,  $A\beta_{1-42}$ , or tau). Although some progress has been made (potential in vivo imaging of  $\alpha$ Syn with the molecule anle138b), more research is needed to optimize these derivatives to propose a suitable and effective fluorescent probe. A way to improve the affinity may be to rationally design compounds able to bind to a specific portion of  $\alpha$ Syn, preferably involved in the core of early-stage aggregates like the pre-NAC or NAC region [172,173]. In this way, a high selectivity and affinity may be expected. Furthermore, by detecting early-stage aggregation, the probe could be of crucial importance in the early diagnosis of neurodegenerative diseases.

### 3.3.2. Radiolabeled Probes

There are a few main characteristics that a compound can bear to be identified as a suitable radiolabeled probe (radiotracer). First, a good affinity (nM scale) and high specificity for  $\alpha$ Syn are required, since  $\alpha$ Syn aggregates in the brain are way less concentrated than other amyloid inclusions (like  $A\beta$  plaques) [174]. Then, these molecules must display appropriate pharmacokinetics properties, such as a suitable lipophilicity ( $\log P = 1-3$ ) and molecular weight (<600 Da). In fact, these optimized parameters allow the compound to cross the BBB and neurons membrane to interact with intracellular  $\alpha$ Syn deposits. Finally, as we saw for the fluorescent probes, they must display a low toxicity profile and an adequate brain clearance, together with chemical stability and a good brain uptake [174]. In the following paragraph, the current development of radiolabeled probes to detect  $\alpha$ Syn aggregation in ex vivo and in vivo systems is presented (see Table 1 for selectivity against a specific amyloid or aggregate type).

Ten years ago, Bagchi et al. synthesized phenothiazine derivatives able to selectively bind to  $\alpha$ Syn fibrils [175,176]. Among them, SIL23 (Figure 3) was the one displaying a moderate affinity for  $\alpha$ Syn fibrils, but had a high selectivity versus  $A\beta$  and tau. By radio-synthesis, the researchers eventually converted the compound into [ $^{125}$ I]SIL23 to create a radiolabeled probe. In vitro binding assays showed that [ $^{125}$ I]SIL23 could bind to  $\alpha$ Syn aggregates in human PD brain homogenates with a  $K_d$  value of  $143 \pm 24$  nM. Also, the compound was able to recognize  $\alpha$ Syn in transgenic PD mice (M83) with a  $K_d$  of 151 nM, but not in healthy controls. The main limit for the further development of this compound was its moderate affinity, which hampered the possibility of performing biodistribution and pharmacokinetic studies [175]. Among the phenothiazine derivatives, other interesting compounds were SIL5 and SIL26, which were also radiolabeled to obtain [ $^{11}$ C]SIL5 (Figure 4) and [ $^{18}$ F]SIL26 [176]. Ex vivo biodistribution studies in rats showed that both [ $^{11}$ C]SIL5 and [ $^{18}$ F]SIL26 (Figure 4) could penetrate the BBB and demonstrated appropriate washout kinetics. However, [ $^{18}$ F]SIL26 was the compound showing the lowest brain uptake, namely a  $0.758 \pm 0.013\%$  injected dose (ID)/g at 5 min after injection. Thus, the only compound suitable for further evaluation was [ $^{11}$ C]SIL5. MicroPET imaging of [ $^{11}$ C]SIL5 in a healthy macaque confirmed that it could cross the BBB and showed a

homogeneous distribution. However, its moderate affinity towards  $\alpha$ Syn fibrils binding, together with a modest brain uptake ( $0.953 \pm 0.115\%$ ID/g), hampered its further application in human PET imaging [175].

In 2015, Chu et al. designed and synthesized a series of 3-benzylidene-indolin-2-one analogues to develop  $\alpha$ Syn PET radiotracers [177]. Among them, compound 46a bore a fluoroethyl side, which could be easily transformed in a  $^{18}\text{F}$  labeled tracer. This molecule, namely [ $^{18}\text{F}$ ]46a (Figure 4), displayed a high affinity for  $\alpha$ Syn fibrils ( $K_d = 2.1 \pm 0.3$  nM) and good selectivity versus A $\beta$  and Tau fibrils ( $K_d = 142.4 \pm 36.9$  nM and  $80.1 \pm 12$  nM, respectively), as displayed by in vitro saturation binding assays [177]. Up to now, [ $^{18}\text{F}$ ]46a is one of the probes with the greatest affinity for  $\alpha$ Syn fibrils [174]. However, when authors tested the capacity of the compound to stain  $\alpha$ Syn fibrils in PD brain slices, they could not obtain a reliable quantification of the detected aggregates. This is probably due to the high  $\log p$  value (4.18) of [ $^{18}\text{F}$ ]46a, which might cause nonspecific binding [177]. Also, further development of this potential probe was hampered by chemical instability issues. In fact, the nitro group might be reduced to the amino group in living systems. Consequently, [ $^{18}\text{F}$ ]46a was not suitable for serving as a PET radiotracer [177].

Radiolabeled diphenyl derivatives were synthesized a few years ago by Ono et al., with the aim of developing  $\alpha$ Syn aggregates ligands [178]. Among them, [ $^{125}\text{I}$ ]IDP-4 (Figure 4) displayed the highest affinity for  $\alpha$ Syn aggregates at  $K_d$  values of  $5.4 \pm 1.5$  nM with a 3-fold selectivity versus A $\beta$  aggregates. Another good hit was [ $^{125}\text{I}$ ]IDP-3, which was able to bind to  $\alpha$ Syn with a  $K_d$  value of  $23.3 \pm 2.8$  nM, as displayed by in vitro binding saturation assays [178]. Notably, fluorescent staining of PD brain sections showed that both compounds could bind to  $\alpha$ Syn aggregates in LBs. However, ex vivo biodistribution in mice showed that [ $^{125}\text{I}$ ]IDP-4 and [ $^{125}\text{I}$ ]IDP-3 (Figure 4) were characterized by a low brain intake. Therefore, neither compound was suitable for in vivo  $\alpha$ Syn imaging [178]. Nevertheless, their capacity to bind to LBs  $\alpha$ Syn aggregates opened the possibility of further chemical modifications on the diphenyl core, which may lead to an increased brain uptake and possible development as a PET imaging probe.

More recently, Verdurand et al. synthesized the benzoxazoles derivatives 2FBox and 4FBox to selectively recognize  $\alpha$ Syn fibrils [179]. The compounds were then radiolabeled with  $^{18}\text{F}$  to assess their suitability as radiotracers. As displayed by in vitro saturation filter binding assays, [ $^{18}\text{F}$ ]2FBox (Figure 4) displayed the highest affinity for  $\alpha$ Syn recombinant fibrils ( $K_d = 3.3 \pm 2.8$  nM). Since the binding assays were promising, the authors decided to further evaluate the compounds using in vitro autoradiography with  $\alpha$ Syn- and A $\beta_{1-42}$  fibril-injected rats, a transgenic PD mice model (M83), and a transgenic AD mice model (PDAPP line J20) [179]. Both compounds could detect A $\beta$  and  $\alpha$ Syn fibrils in a non-selective manner in the fibrils-injected rats, but failed to recognize A $\beta_{1-42}$  and  $\alpha$ Syn aggregates in the other mice models [174,179]. To obtain more insights on the activity of those candidates towards amyloid aggregates' detection, the authors carried out imaging experiments on post mortem brain sections (PD, MSA, and AD patients). Surprisingly, neither [ $^{18}\text{F}$ ]2FBox or [ $^{18}\text{F}$ ]4FBox (Table 1) could detect A $\beta_{1-42}$  and  $\alpha$ Syn aggregates, while in vivo PET imaging of rats showed that the compounds could cross the BBB with a good initial brain uptake but failed to detect amyloids fibrils in the fibril-injected rats. Due to these limitations, namely amyloid non-selectivity and a lack of aggregate detection ex vivo and in vivo, [ $^{18}\text{F}$ ]2FBox and [ $^{18}\text{F}$ ]4FBox were not suitable as PET radiotracers for  $\alpha$ Syn [179].

Anle253b is a diphenyl pyrazole sharing a similar structure with that of anle138b [168], identified by Maurer et al. as a possible PET tracer. Bearing an accessible methyl group, the compound was suitable for  $^{11}\text{C}$  methylation; thus, it was selected and screened as a PET imaging probe. Interestingly, anle253b bound to  $\alpha$ Syn fibrils with an  $\text{IC}_{50}$  value of 1.6 nM. This very good affinity profile pushed the authors to perform in vivo PET studies in healthy rats [180]. These experiments showed that [ $^{11}\text{C}$ ]anle253b (Figure 4) could cross the BBB with medium brain uptake and was distributed homogeneously in the rat brain. However, data regarding its uptake dynamics, as well as selectivity versus other amyloid aggregates, have yet to be collected and optimized. In particular, the compound displayed a high lipophilic-

ity ( $\log P = 5.21$ ), which may be responsible for the poor pharmacokinetics of [ $^{11}\text{C}$ ]anle253b in vivo. Thus, although the preliminary data regarding the brain uptake and bioavailability of [ $^{11}\text{C}$ ]anle253b are promising, at the current stage, it cannot be employed as a PET tracer in humans [174,181]. The optimization of anle253b, in particular the replacement of a phenyl ring with pyridine to decrease the compound's lipophilicity, led to MODAG-001 [182]. To make the compound suitable for PET imaging scanning, Kuebler et al. radiolabeled MODAG-001 with  $^3\text{H}$  and  $^{11}\text{C}$  [182] (Table 1). Thus, the researchers carried out a series of in vitro and in vivo biological evaluation studies with both [ $^{11}\text{C}$ ]MODAG-001 and [ $^3\text{H}$ ]MODAG-001. In particular, [ $^3\text{H}$ ]MODAG-001 displayed an impressive high binding affinity for  $\alpha\text{Syn}$  fibrils in vitro, with a  $K_d$  value of 0.6 nM. Furthermore, it showed a 30-fold selectivity over Tau and  $\text{A}\beta_{1-42}$  aggregates [181]. Additionally, [ $^{11}\text{C}$ ]MODAG-001 was able to efficiently penetrate the mouse brain ( $\text{SUV} = 1.4$ ). Interestingly, thanks to metabolic studies, the authors noticed that one of the three main metabolites of [ $^{11}\text{C}$ ]MODAG-001 was represented by the demethylated derivative. Thus, being afraid that demethylation might hamper PET quantification imaging, the researchers fully deuterated the nonradioactive methyl group and synthesized (d3)-[ $^{11}\text{C}$ ]MODAG-001. By in vivo PET imaging, the authors evaluated the binding properties of (d3)-[ $^{11}\text{C}$ ]MODAG-001 in three  $\alpha\text{Syn}$ -fibril-inoculated rats and one noninjected control. Interestingly, significantly higher signals were observed in the three  $\alpha\text{Syn}$ -fibril-inoculated rats at 4 days after (d3)-[ $^{11}\text{C}$ ]MODAG-001 injection [182]. This was indicative of the compound's good binding profile towards  $\alpha\text{Syn}$  aggregates. To further characterize (d3)-[ $^{11}\text{C}$ ]MODAG-001 as a possible PET tracer, the researchers carried out in vitro autoradiography in LBD (Lewy Bodies Dementia), PSP (Progressive Supranuclear Palsy), AD, and healthy control cases. Surprisingly, no strong binding was observed in any of the LBD brain sections, but  $\text{A}\beta$  plaques were observed in the AD brain tissues [174,182]. Furthermore, no Tau fibrils were shown in the PSP and AD cases. This can be explained in terms of non-specific binding and low target availability in LBD brains.

Recently, Kaide et al. designed and synthesized bis-quinoline derivatives as useful probes for in vivo  $\alpha\text{Syn}$  imaging [183]. To assess the activity of these derivatives in detecting  $\alpha\text{Syn}$  aggregates, the authors first performed competitive inhibition assays in vitro. Notably, two compounds (BQ-1 and BQ-2) showed a high affinity towards  $\alpha\text{Syn}$  fibrils ( $K_i$  equal to 17.0 and 11.6 nM, respectively) [183]. Interestingly, fluorescent staining experiments proved the efficacy of BQ-1 and BQ-2 in detecting  $\alpha\text{Syn}$  aggregates in PD human brain samples. Since BQ-2 showed the highest affinity towards  $\alpha\text{Syn}$  aggregates, it was chosen for radiolabeling and further evaluations. Thus, the authors evaluated the lipophilicity of [ $^{18}\text{F}$ ]BQ-2 (Figure 4) and performed biodistribution studies in vivo (mice). Interestingly, the compound displayed a moderate initial brain uptake (1.59%ID/g at 2 min postinjection) and was characterized by a moderate  $\log D$  (2.62) [183]. Despite its promising pharmacokinetic profile, [ $^{18}\text{F}$ ]BQ-2 was primarily retained in the brain (1.35%ID/g at 60 min postinjection), probably because of nonspecific binding. This disadvantage was confirmed by in vitro autoradiography. In fact, a large amount of nonspecific binding was observed in the whole brain section [183]. Finally, this suggests that [ $^{18}\text{F}$ ]BQ-2 was not a suitable PET probe for imaging  $\alpha\text{Syn}$  aggregates in PD patients' brains.

In comparison with fluorescent probes developed for the imaging of  $\alpha\text{Syn}$  in ex vivo and in vivo samples, the research on radiolabeled probes has taken several steps forward. In fact, [ $^{125}\text{I}$ ]IDP-3 and [ $^{125}\text{I}$ ]IDP-4 were able to stain  $\alpha\text{Syn}$  in LB ex vivo samples, while other candidates like [ $^3\text{H}$ ]MODAG-001 and [ $^{18}\text{F}$ ]46a were characterized by a potent affinity for  $\alpha\text{Syn}$  fibrils [177,178,182]. Furthermore, most of the compounds discussed in this paragraph were able to cross the BBB and spread homogeneously in the brains of in vivo models. However, no suitable radiolabeled probe has yet been obtained for  $\alpha\text{Syn}$  imaging. The main limits are represented by a low brain uptake, low amyloid selectivity, chemical instability, and low affinity for specific  $\alpha\text{Syn}$  species [174]. As a result, more efforts are required to develop a suitable compound able to be exploited as an  $\alpha\text{Syn}$  imaging probe [180].

#### 4. Conclusions

The lack of early diagnoses of neurodegenerative diseases (e.g., AD and PD) underscores the critical need for inexpensive, easy-to-access probes able to detect the early onset of the pathologies. While relevant variations in biomarkers of specific proteinopathies have been identified even several years before the onset of the disease, to date, the clinical diagnosis of most of neurodegenerative disease relies on PET or MRI imaging. However, the application of such techniques presents several limitations. These include the high costs related to the analyses, the risks to health for patients that are continuously under monitoring, and, in some cases, the low accuracy in discriminating among the different neurodegenerative diseases. In addition, only post mortem analyses performed on patients' brain tissues are able to correctly discriminate between different pathologies [4]. Furthermore, current diagnostic methods employing imaging technologies and biofluid analysis still encounter challenges, often related to low detectability and invasiveness issues. However, much progress has been made in recent years regarding  $A\beta_{1-42}$  imaging, in particular towards the detection of early toxic aggregation species such as oligomers, for example through the identification of novel and more effective probes. Examples in this respect come from the fluorescent, aromatic BD-Oligo and PTO-29 probes, which showed good photophysical properties, a high selectivity towards proteins oligomers, good blood–brain barrier penetration, low cytotoxicity, and successful in vivo imaging in mouse models [77,79]. Additionally, the fluoro-cyanine probe F-SLOH demonstrated a good  $A\beta$  oligomer selectivity with a high binding affinity ex vivo and in vivo [81]. However, data are still missing regarding their selectivity towards different amyloid proteins and neurodegenerative diseases. Similar considerations arise also for Tau species. Indeed, significant advancements have been observed in both biomarkers monitoring and in the field of PET and fluorescent probe imaging in recent years. With regard to biomarkers monitoring, most of the progress observed so far has come from the introduction of techniques enabling the identification of Tau species in large populations of patients, in non-invasive fluids, and the simultaneous monitoring of multiple Tau-related biomarkers. In addition, the discovery of PET tracers such as [ $^{18}\text{F}$ ]-MK-6240, [ $^{18}\text{F}$ ]-PI-2620, [ $^{18}\text{F}$ ]-RO-948, and [ $^{18}\text{F}$ ]-APN-1607 has enabled the discrimination of AD patients from controls, as displayed by in vivo studies [131–134]. Similarly, fluorescent probes such as Q-Tau 1 to 4, pTP-TFE and BT1 showed a low toxicity and high affinity for Tau aggregates towards  $A\beta_{1-42}$  [157,161,164]. However, it should be pointed out that the above-mentioned PET probes displayed low brain permeability, and the latter fluorescent ones were tested only in ex vivo samples. Thus, their development for human in vivo imaging has yet to be challenged. Finally, regarding  $\alpha\text{Syn}$ , fluorescent probes able to detect early-stage aggregates ex vivo or in vivo are still in their infancy and require a drastic optimization. In fact, only Anle138b showed good results in detecting oligomers and fibrils in vivo, but its lack of selectivity towards different amyloid species stopped it from further development [168]. Regarding radiolabeled probes, some progress has been made in the PET imaging field. For example, the probe [ $^{11}\text{C}$ ]-SIL5 showed good brain penetration and favorable pharmacokinetics properties, but had a modest selectivity for  $\alpha\text{Syn}$  high-ordered aggregates (fibrils) [175]. On the contrary, compounds BQ-1 and BQ-2 displayed a high selectivity for  $\alpha\text{Syn}$  fibrils, but a low brain uptake [183]. Again, these limitations hampered the development of these molecules for the early diagnosis of neurodegenerative diseases [180].

Even if the advent of near-infrared fluorescent probes presents a promising avenue for the non-invasive visualization of amyloid aggregates, challenges in specificity, selectivity, and clinical translation persist, urging further exploration into new chemical biology tools and probes. In this review, we offered a nuanced assessment of the achievements, drawbacks, and potential directions in the development of fluorescent and radiolabelled probes for neurodegenerative disease diagnosis. By critically evaluating the current state of the art, this review aims to propel advancements in neuropathology, steering toward preventive measures and early diagnosis with enhanced precision and accessibility in the realm of neurodegenerative diseases.



**Author Contributions:** Conceptualization, N.B. and N.T.; writing—original draft preparation, L.P., N.B. and N.T.; writing—review and editing, G.R., L.P., N.B. and N.T.; supervision, N.B. and N.T. All authors have read and agreed to the published version of the manuscript.

**Funding:** This research was funded by FAR—Fondo di Ateneo per la Ricerca 2019 (grant number 166835) and by Banca Popolare dell’Emilia-Romagna (BPER) (G.R.). L.P. would like to thank the Italian funding program Fondo Sociale Europeo REACT-EU—PON “Ricerca e Innovazione” 2014–2020—Azione IV.4 “Dottorati e contratti di ricerca su tematiche dell’innovazione” (CUP: E95F21002320001; contract number: 17-I-13884-1) for supporting his research. N.T. would like to thank the PRCI DFG-ANR funding program (FluPepDye “Development of new peptide based NIR probe conjugates for specifically and selectively detecting amyloid early biomarkers” ANR-22-CE92-0076) for supporting his research. TubInTrain project is thanked for the PhD funding for N.B. The TubInTrain project has received funding from the European Union’s Horizon 2020 research and innovation program under the Marie Skłodowska-Curie grant agreement No 860070. The APC was funded by MDPI.

**Institutional Review Board Statement:** Not applicable.

**Informed Consent Statement:** Not applicable.

**Data Availability Statement:** Not applicable.

**Conflicts of Interest:** The authors declare no conflicts of interest.

## References

1. Key Figures. Available online: <https://institutducerveau-icm.org/en/key-figures/> (accessed on 21 November 2022).
2. Erkkinen, M.G.; Kim, M.-O.; Geschwind, M.D. Clinical Neurology and Epidemiology of the Major Neurodegenerative Diseases. *Cold Spring Harb. Perspect. Biol.* **2018**, *10*, a033118. [[CrossRef](#)]
3. Spillantini, M.G.; Crowther, R.A.; Jakes, R.; Hasegawa, M.; Goedert, M. A-Synuclein in Filamentous Inclusions of Lewy Bodies from Parkinson’s Disease and Dementia with Lewy Bodies. *Proc. Natl. Acad. Sci. USA* **1998**, *95*, 6469–6473. [[CrossRef](#)]
4. Karran, E.; De Strooper, B. The Amyloid Hypothesis in Alzheimer Disease: New Insights from New Therapeutics. *Nat. Rev. Drug Discov.* **2022**, *21*, 306–318. [[CrossRef](#)]
5. Xu, M.; Ryan, P.; Rudrawar, S.; Quinn, R.J.; Zhang, H.; Mellick, G.D. Advances in the Development of Imaging Probes and Aggregation Inhibitors for Alpha-Synuclein. *Acta Pharmacol. Sin.* **2020**, *41*, 483–498. [[CrossRef](#)]
6. Morris, E.; Chalkidou, A.; Hammers, A.; Peacock, J.; Summers, J.; Keevil, S. Diagnostic Accuracy of <sup>18</sup>F Amyloid PET Tracers for the Diagnosis of Alzheimer’s Disease: A Systematic Review and Meta-Analysis. *Eur. J. Nucl. Med. Mol. Imaging* **2016**, *43*, 374–385. [[CrossRef](#)]
7. Herholz, K.; Ebmeier, K. Clinical Amyloid Imaging in Alzheimer’s Disease. *Lancet Neurol.* **2011**, *10*, 667–670. [[CrossRef](#)]
8. Stenh, C.; Englund, H.; Lord, A.; Johansson, A.-S.; Almeida, C.G.; Gellerfors, P.; Greengard, P.; Gouras, G.K.; Lannfelt, L.; Nilsson, L.N.G. Amyloid- $\beta$  Oligomers Are Inefficiently Measured by Enzyme-Linked Immunosorbent Assay. *Ann. Neurol.* **2005**, *58*, 147–150. [[CrossRef](#)]
9. Hong, M.C.; Kim, Y.K.; Choi, J.Y.; Yang, S.Q.; Rhee, H.; Ryu, Y.H.; Choi, T.H.; Cheon, G.J.; An, G.I.; Kim, H.Y.; et al. Synthesis and Evaluation of Stilbene Derivatives as a Potential Imaging Agent of Amyloid Plaques. *Bioorganic Med. Chem.* **2010**, *18*, 7724–7730. [[CrossRef](#)]
10. Sehlin, D.; Söllvander, S.; Paulie, S.; Brundin, R.; Ingelsson, M.; Lannfelt, L.; Pettersson, F.E.; Englund, H. Interference from Heterophilic Antibodies in Amyloid- $\beta$  Oligomer ELISAs. *J. Alzheimer’s Dis. JAD* **2010**, *21*, 1295–1301. [[CrossRef](#)]
11. Mattsson, N.; Lönneborg, A.; Boccardi, M.; Blennow, K.; Hansson, O. Geneva Task Force for the Roadmap of Alzheimer’s Biomarkers Clinical Validity of Cerebrospinal Fluid A $\beta$ 42, Tau, and Phospho-Tau as Biomarkers for Alzheimer’s Disease in the Context of a Structured 5-Phase Development Framework. *Neurobiol. Aging* **2017**, *52*, 196–213. [[CrossRef](#)]
12. Shahnawaz, M.; Mukherjee, A.; Pritzkow, S.; Mendez, N.; Rabadia, P.; Liu, X.; Hu, B.; Schmeichel, A.; Singer, W.; Wu, G.; et al. Discriminating  $\alpha$ -Synuclein Strains in Parkinson’s Disease and Multiple System Atrophy. *Nature* **2020**, *578*, 273–277. [[CrossRef](#)]
13. Schöll, M.; Maass, A.; Mattsson, N.; Ashton, N.J.; Blennow, K.; Zetterberg, H.; Jagust, W. Biomarkers for Tau Pathology. *Mol. Cell. Neurosci.* **2019**, *97*, 18–33. [[CrossRef](#)]
14. Schraen-Maschke, S.; Sergeant, N.; Dhaenens, C.-M.; Bombois, S.; Deramecourt, V.; Caillet-Boudin, M.-L.; Pasquier, F.; Muraige, C.-A.; Sablonnière, B.; Vanmechelen, E.; et al. Tau as a Biomarker of Neurodegenerative Diseases. *Biomark. Med.* **2008**, *2*, 363–384. [[CrossRef](#)]
15. Blennow, K.; Hampel, H. CSF Markers for Incipient Alzheimer’s Disease. *Lancet Neurol.* **2003**, *2*, 605–613. [[CrossRef](#)]
16. Wallin, Å.K.; Blennow, K.; Zetterberg, H.; Londos, E.; Minthon, L.; Hansson, O. CSF Biomarkers Predict a More Malignant Outcome in Alzheimer Disease. *Neurology* **2010**, *74*, 1531–1537. [[CrossRef](#)]
17. Buchhave, P.; Minthon, L.; Zetterberg, H.; Wallin, Å.K.; Blennow, K.; Hansson, O. Cerebrospinal Fluid Levels Of  $\beta$ -Amyloid 1–42, but Not of Tau, Are Fully Changed Already 5 to 10 Years Before the Onset of Alzheimer Dementia. *Arch. General. Psychiatry* **2012**, *69*, 98–106. [[CrossRef](#)]



18. Luk, C.; Compta, Y.; Magdalino, N.; Martí, M.J.; Hondhamuni, G.; Zetterberg, H.; Blennow, K.; Constantinescu, R.; Pijnenburg, Y.; Mollenhauer, B.; et al. Development and Assessment of Sensitive Immuno-PCR Assays for the Quantification of Cerebrospinal Fluid Three- and Four-Repeat Tau Isoforms in Tauopathies. *J. Neurochem.* **2012**, *123*, 396–405. [[CrossRef](#)]
19. Barthélemy, N.R.; Fenaille, F.; Hirtz, C.; Sergeant, N.; Schraen-Maschke, S.; Vialaret, J.; Buée, L.; Gabelle, A.; Junot, C.; Lehmann, S.; et al. Tau Protein Quantification in Human Cerebrospinal Fluid by Targeted Mass Spectrometry at High Sequence Coverage Provides Insights into Its Primary Structure Heterogeneity. *J. Proteome Res.* **2016**, *15*, 667–676. [[CrossRef](#)]
20. Ashton, N.J.; Hye, A.; Rajkumar, A.P.; Leuzy, A.; Snowden, S.; Suárez-Calvet, M.; Karikari, T.K.; Schöll, M.; La Joie, R.; Rabinovici, G.D.; et al. An Update on Blood-Based Biomarkers for Non-Alzheimer Neurodegenerative Disorders. *Nat. Rev. Neurol.* **2020**, *16*, 265–284. [[CrossRef](#)]
21. Karikari, T.K.; Ashton, N.J.; Brinkmalm, G.; Brum, W.S.; Benedet, A.L.; Montoliu-Gaya, L.; Lantero-Rodriguez, J.; Pascoal, T.A.; Suárez-Calvet, M.; Rosa-Neto, P.; et al. Blood Phospho-Tau in Alzheimer Disease: Analysis, Interpretation, and Clinical Utility. *Nat. Rev. Neurol.* **2022**, *18*, 400–418. [[CrossRef](#)]
22. Kac, P.R.; Gonzalez-Ortiz, F.; Simrén, J.; Dewit, N.; Vanmechelen, E.; Zetterberg, H.; Blennow, K.; Ashton, N.J.; Karikari, T.K. Diagnostic Value of Serum versus Plasma Phospho-Tau for Alzheimer’s Disease. *Alzheimer’s Res. Ther.* **2022**, *14*, 65. [[CrossRef](#)]
23. Karikari, T.K.; Pascoal, T.A.; Ashton, N.J.; Janelidze, S.; Benedet, A.L.; Rodriguez, J.L.; Chamoun, M.; Savard, M.; Kang, M.S.; Therriault, J.; et al. Blood Phosphorylated Tau 181 as a Biomarker for Alzheimer’s Disease: A Diagnostic Performance and Prediction Modelling Study Using Data from Four Prospective Cohorts. *Lancet Neurol.* **2020**, *19*, 422–433. [[CrossRef](#)]
24. Janelidze, S.; Mattsson, N.; Palmqvist, S.; Smith, R.; Beach, T.G.; Serrano, G.E.; Chai, X.; Proctor, N.K.; Eichenlaub, U.; Zetterberg, H.; et al. Plasma P-Tau181 in Alzheimer’s Disease: Relationship to Other Biomarkers, Differential Diagnosis, Neuropathology and Longitudinal Progression to Alzheimer’s Dementia. *Nat. Med.* **2020**, *26*, 379–386. [[CrossRef](#)]
25. Mielke, M.M.; Hagen, C.E.; Xu, J.; Chai, X.; Vemuri, P.; Lowe, V.J.; Airey, D.C.; Knopman, D.S.; Roberts, R.O.; Machulda, M.M.; et al. Plasma Phospho-Tau181 Increases with Alzheimer’s Disease Clinical Severity and Is Associated with Tau-PET and Amyloid-PET. *Alzheimer’s Dement.* **2018**, *14*, 989–997. [[CrossRef](#)]
26. Ashton, N.J.; Pascoal, T.A.; Karikari, T.K.; Benedet, A.L.; Lantero-Rodriguez, J.; Brinkmalm, G.; Snellman, A.; Schöll, M.; Troakes, C.; Hye, A.; et al. Plasma P-Tau231: A New Biomarker for Incipient Alzheimer’s Disease Pathology. *Acta Neuropathol.* **2021**, *141*, 709–724. [[CrossRef](#)]
27. Thijssen, E.H.; La Joie, R.; Wolf, A.; Strom, A.; Wang, P.; Iaccarino, L.; Bourakova, V.; Cobigo, Y.; Heuer, H.; Spina, S.; et al. Diagnostic Value of Plasma Phosphorylated Tau181 in Alzheimer’s Disease and Frontotemporal Lobar Degeneration. *Nat. Med.* **2020**, *26*, 387–397. [[CrossRef](#)]
28. Palmqvist, S.; Janelidze, S.; Quiroz, Y.T.; Zetterberg, H.; Lopera, F.; Stomrud, E.; Su, Y.; Chen, Y.; Serrano, G.E.; Leuzy, A.; et al. Discriminative Accuracy of Plasma Phospho-Tau217 for Alzheimer Disease vs Other Neurodegenerative Disorders. *JAMA* **2020**, *324*, 772–781. [[CrossRef](#)]
29. Bayoumy, S.; Verberk, I.M.W.; den Dulk, B.; Hussaini, Z.; Zwan, M.; van der Flier, W.M.; Ashton, N.J.; Zetterberg, H.; Blennow, K.; Vanbrabant, J.; et al. Clinical and Analytical Comparison of Six Simoa Assays for Plasma P-Tau Isoforms P-Tau181, P-Tau217, and P-Tau231. *Alzheimer’s Res. Ther.* **2021**, *13*, 198. [[CrossRef](#)]
30. Ossenkoppele, R.; van der Kant, R.; Hansson, O. Tau Biomarkers in Alzheimer’s Disease: Towards Implementation in Clinical Practice and Trials. *Lancet Neurol.* **2022**, *21*, 726–734. [[CrossRef](#)]
31. Balhara, N.; Devi, M.; Balda, A.; Phour, M.; Giri, A. Urine; a New Promising Biological Fluid to Act as a Non-Invasive Biomarker for Different Human Diseases. *URINE* **2023**, *5*, 40–52. [[CrossRef](#)]
32. Harpole, M.; Davis, J.; Espina, V. Current State of the Art for Enhancing Urine Biomarker Discovery. *Expert. Rev. Proteom.* **2016**, *13*, 609–626. [[CrossRef](#)]
33. Kohlhase, K.; Frank, F.; Wilmes, C.; Koerbel, K.; Schaller-Paule, M.A.; Miles, M.; Betz, C.; Steinmetz, H.; Foerch, C. Brain-Specific Biomarkers in Urine as a Non-Invasive Approach to Monitor Neuronal and Glial Damage. *Eur. J. Neurol.* **2023**, *30*, 729–740. [[CrossRef](#)]
34. Shi, M.; Sui, Y.-T.; Peskind, E.R.; Li, G.; Hwang, H.; Devic, I.; Gingham, C.; Edgar, J.S.; Pan, C.; Goodlett, D.R.; et al. Salivary Tau Species Are Potential Biomarkers of Alzheimer’s Disease. *J. Alzheimer’s Dis.* **2011**, *27*, 299–305. [[CrossRef](#)]
35. Marksteiner, J.; Defrancesco, M.; Humpel, C. Saliva Tau and Phospho-Tau-181 Measured by Lumipulse in Patients with Alzheimer’s Disease. *Front. Aging Neurosci.* **2022**, *14*, 1014305. [[CrossRef](#)]
36. Pekeles, H.; Qureshi, H.Y.; Paudel, H.K.; Schipper, H.M.; Gornistky, M.; Chertkow, H. Development and Validation of a Salivary Tau Biomarker in Alzheimer’s Disease. *Alzheimer’s Dement.* **2018**, *11*, 53–60. [[CrossRef](#)]
37. Ashton, N.J.; Schöll, M.; Heurling, K.; Gkanatsiou, E.; Portelius, E.; Höglund, K.; Brinkmalm, G.; Hye, A.; Blennow, K.; Zetterberg, H. Update on Biomarkers for Amyloid Pathology in Alzheimer’s Disease. *Biomark. Med.* **2018**, *12*, 799–812. [[CrossRef](#)]
38. Sabaei, M.; Rahimian, S.; Haj Mohamad Ebrahim Ketabforoush, A.; Rasoolijazi, H.; Zamani, B.; Hajiakhoundi, F.; Soleimani, M.; Shahidi, G.; Faramarzi, M. Salivary Levels of Disease-Related Biomarkers in the Early Stages of Parkinson’s and Alzheimer’s Disease: A Cross-Sectional Study. *IBRO Neurosci. Rep.* **2023**, *14*, 285–292. [[CrossRef](#)]
39. Lau, H.-C.; Lee, I.-K.; Ko, P.-W.; Lee, H.-W.; Huh, J.-S.; Cho, W.-J.; Lim, J.-O. Non-Invasive Screening for Alzheimer’s Disease by Sensing Salivary Sugar Using *Drosophila* Cells Expressing Gustatory Receptor (Gr5a) Immobilized on an Extended Gate Ion-Sensitive Field-Effect Transistor (EG-ISFET) Biosensor. *PLoS ONE* **2015**, *10*, e0117810. [[CrossRef](#)]

40. Ashton, N.J.; Ide, M.; Zetterberg, H.; Blennow, K. Salivary Biomarkers for Alzheimer's Disease and Related Disorders. *Neurol. Ther.* **2019**, *8*, 83–94. [[CrossRef](#)]
41. Dame, Z.T.; Aziat, F.; Mandal, R.; Krishnamurthy, R.; Bouatra, S.; Borzouie, S.; Guo, A.C.; Sajed, T.; Deng, L.; Lin, H.; et al. The Human Saliva Metabolome. *Metabolomics* **2015**, *11*, 1864–1883. [[CrossRef](#)]
42. Król-Grzymała, A.; Sienkiewicz-Szłapka, E.; Fiedorowicz, E.; Rozmus, D.; Cieślińska, A.; Grzybowski, A. Tear Biomarkers in Alzheimer's and Parkinson's Diseases, and Multiple Sclerosis: Implications for Diagnosis (Systematic Review). *Int. J. Mol. Sci.* **2022**, *23*, 10123. [[CrossRef](#)]
43. Gijs, M.; Ramakers, I.H.G.B.; Visser, P.J.; Verhey, F.R.J.; van de Waarenburg, M.P.H.; Schalkwijk, C.G.; Nuijts, R.M.M.A.; Webers, C.A.B. Association of Tear Fluid Amyloid and Tau Levels with Disease Severity and Neurodegeneration. *Sci. Rep.* **2021**, *11*, 22675. [[CrossRef](#)]
44. Gharbiya, M.; Visioli, G.; Trebbastoni, A.; Albanese, G.M.; Colardo, M.; D'Antonio, F.; Segatto, M.; Lambiase, A. Beta-Amyloid Peptide in Tears: An Early Diagnostic Marker of Alzheimer's Disease Correlated with Choroidal Thickness. *Int. J. Mol. Sci.* **2023**, *24*, 2590. [[CrossRef](#)]
45. Ohm, T.G.; Braak, H. Olfactory Bulb Changes in Alzheimer's Disease. *Acta Neuropathol.* **1987**, *73*, 365–369. [[CrossRef](#)]
46. Attems, J.; Jellinger, K.A. Olfactory Tau Pathology in Alzheimer Disease and Mild Cognitive Impairment. *Clin. Neuropathol.* **2006**, *25*, 265–271.
47. Passali, G.C.; Politi, L.; Crisanti, A.; Loglisci, M.; Anzivino, R.; Passali, D. Tau Protein Detection in Anosmic Alzheimer's Disease Patient's Nasal Secretions. *Chemodosens. Percept.* **2015**, *8*, 201–206. [[CrossRef](#)]
48. Pahrudin Arrozi, A.; Yanagisawa, D.; Kato, T.; Akatsu, H.; Hashizume, Y.; Kaneda, D.; Tooyama, I. Nasal Extracts from Patients with Alzheimer's Disease Induce Tau Aggregates in a Cellular Model of Tau Propagation. *J. Alzheimer's Dis. Rep.* **2021**, *5*, 263–274. [[CrossRef](#)]
49. Lee, D.; Kim, S.M.; Kim, H.Y.; Kim, Y. Fluorescence Chemicals To Detect Insoluble and Soluble Amyloid- $\beta$  Aggregates. *ACS Chem. Neurosci.* **2019**, *10*, 2647–2657. [[CrossRef](#)]
50. Zhou, Y.; Hua, J.; Ding, D.; Tang, Y. Interrogating Amyloid Aggregation with Aggregation-Induced Emission Fluorescence Probes. *Biomaterials* **2022**, *286*, 121605. [[CrossRef](#)]
51. Wang, Y.; Chen, J.; Gao, F.; Hu, M.; Wang, X. Recent Developments in the Chemical Biology of Amyloid- $\beta$  Oligomer Targeting. *Org. Biomol. Chem.* **2023**, *21*, 4540–4552. [[CrossRef](#)]
52. Li, Q.; Lee, J.-S.; Ha, C.; Park, C.B.; Yang, G.; Gan, W.B.; Chang, Y.-T. Solid-Phase Synthesis of Styryl Dyes and Their Application as Amyloid Sensors. *Angew. Chem. Int. Ed. Engl.* **2004**, *43*, 6331–6335. [[CrossRef](#)]
53. Li, Q.; Min, J.; Ahn, Y.-H.; Namm, J.; Kim, E.M.; Lui, R.; Kim, H.Y.; Ji, Y.; Wu, H.; Wisniewski, T.; et al. Styryl-Based Compounds as Potential in Vivo Imaging Agents for Beta-Amyloid Plaques. *Chembiochem* **2007**, *8*, 1679–1687. [[CrossRef](#)]
54. Staderini, M.; Aulić, S.; Bartolini, M.; Tran, H.N.A.; González-Ruiz, V.; Pérez, D.I.; Cabezas, N.; Martínez, A.; Martín, M.A.; Andrisano, V.; et al. A Fluorescent Styrylquinoline with Combined Therapeutic and Diagnostic Activities against Alzheimer's and Prion Diseases. *ACS Med. Chem. Lett.* **2013**, *4*, 225–229. [[CrossRef](#)]
55. Lee, C.-J.; Sheu, C.-N.; Tsai, C.-C.; Wu, Z.-Z.; Lin, W. Direct  $\beta$ -Acylation of 2-Arylidene-1,3-Indandiones with Acyl Chlorides Catalyzed by Organophosphanes. *Chem. Commun.* **2014**, *50*, 5304–5306. [[CrossRef](#)]
56. Hintersteiner, M.; Enz, A.; Frey, P.; Jatón, A.-L.; Kinzy, W.; Kneuer, R.; Neumann, U.; Rudin, M.; Staufienbiel, M.; Stoekli, M.; et al. In Vivo Detection of Amyloid-Beta Deposits by near-Infrared Imaging Using an Oxazine-Derivative Probe. *Nat. Biotechnol.* **2005**, *23*, 577–583. [[CrossRef](#)]
57. Nesterov, E.E.; Skoch, J.; Hyman, B.T.; Klunk, W.E.; Bacskai, B.J.; Swager, T.M. In Vivo Optical Imaging of Amyloid Aggregates in Brain: Design of Fluorescent Markers. *Angew. Chem. Int. Ed.* **2005**, *44*, 5452–5456. [[CrossRef](#)]
58. Raymond, S.B.; Skoch, J.; Hills, I.D.; Nesterov, E.E.; Swager, T.M.; Bacskai, B.J. Smart Optical Probes for Near-Infrared Fluorescence Imaging of Alzheimer's Disease Pathology. *Eur. J. Nucl. Med. Mol. Imaging* **2008**, *35* (Suppl. 1), S93–S98. [[CrossRef](#)]
59. Zhang, X.; Tian, Y.; Li, Z.; Tian, X.; Sun, H.; Liu, H.; Moore, A.; Ran, C. Design and Synthesis of Curcumin Analogues for in Vivo Fluorescence Imaging and Inhibiting Copper-Induced Cross-Linking of Amyloid Beta Species in Alzheimer's Disease. *J. Am. Chem. Soc.* **2013**, *135*, 16397–16409. [[CrossRef](#)]
60. Liu, K.; Guo, T.L.; Chojnacki, J.; Lee, H.-G.; Wang, X.; Siedlak, S.L.; Rao, W.; Zhu, X.; Zhang, S. Bivalent Ligand Containing Curcumin and Cholesterol as Fluorescence Probe for A $\beta$  Plaques in Alzheimer's Disease. *ACS Chem. Neurosci.* **2012**, *3*, 141–146. [[CrossRef](#)]
61. Ran, C.; Xu, X.; Raymond, S.B.; Ferrara, B.J.; Neal, K.; Bacskai, B.J.; Medarova, Z.; Moore, A. Design, Synthesis, and Testing of Difluoroboron-Derivatized Curcumins as Near-Infrared Probes for in Vivo Detection of Amyloid- $\beta$  Deposits. *J. Am. Chem. Soc.* **2009**, *131*, 15257–15261. [[CrossRef](#)]
62. Ono, M.; Ishikawa, M.; Kimura, H.; Hayashi, S.; Matsumura, K.; Watanabe, H.; Shimizu, Y.; Cheng, Y.; Cui, M.; Kawashima, H.; et al. Development of Dual Functional SPECT/Fluorescent Probes for Imaging Cerebral Beta-Amyloid Plaques. *Bioorganic Med. Chem. Lett.* **2010**, *20*, 3885–3888. [[CrossRef](#)]
63. Jung, S.-J.; Park, S.-H.; Lee, E.J.; Park, J.H.; Kong, Y.B.; Rho, J.K.; Hur, M.G.; Yang, S.D.; Park, Y.D. Development of Fluorescent Probes That Bind and Stain Amyloid Plaques in Alzheimer's Disease. *Arch. Pharmacol. Res.* **2015**, *38*, 1992–1998. [[CrossRef](#)]

64. Neo Shin, N.; Jeon, H.; Jung, Y.; Baek, S.; Lee, S.; Yoo, H.C.; Bae, G.H.; Park, K.; Yang, S.-H.; Han, J.M.; et al. Fluorescent 1,4-Naphthoquinones To Visualize Diffuse and Dense-Core Amyloid Plaques in APP/PS1 Transgenic Mouse Brains. *ACS Chem. Neurosci.* **2019**, *10*, 3031–3044. [[CrossRef](#)]
65. Ono, M.; Watanabe, H.; Kimura, H.; Saji, H. BODIPY-Based Molecular Probe for Imaging of Cerebral  $\beta$ -Amyloid Plaques. *ACS Chem. Neurosci.* **2012**, *3*, 319–324. [[CrossRef](#)]
66. Ulrich, G.; Ziesel, R.; Harriman, A. The Chemistry of Fluorescent Bodipy Dyes: Versatility Unsurpassed. *Angew. Chem. Int. Ed.* **2008**, *47*, 1184–1201. [[CrossRef](#)] [[PubMed](#)]
67. Boens, N.; Leen, V.; Dehaen, W. Fluorescent Indicators Based on BODIPY. *Chem. Soc. Rev.* **2012**, *41*, 1130–1172. [[CrossRef](#)] [[PubMed](#)]
68. Smith, N.W.; Alonso, A.; Brown, C.M.; Dzyuba, S.V. Triazole-Containing BODIPY Dyes as Novel Fluorescent Probes for Soluble Oligomers of Amyloid A $\beta$ 1–42 Peptide. *Biochem. Biophys. Res. Commun.* **2010**, *391*, 1455–1458. [[CrossRef](#)] [[PubMed](#)]
69. Ren, W.; Zhang, J.; Peng, C.; Xiang, H.; Chen, J.; Peng, C.; Zhu, W.; Huang, R.; Zhang, H.; Hu, Y. Fluorescent Imaging of  $\beta$ -Amyloid Using BODIPY Based Near-Infrared Off-On Fluorescent Probe. *Bioconjugate Chem.* **2018**, *29*, 3459–3466. [[CrossRef](#)] [[PubMed](#)]
70. Fu, H.; Cui, M.; Zhao, L.; Tu, P.; Zhou, K.; Dai, J.; Liu, B. Highly Sensitive Near-Infrared Fluorophores for in Vivo Detection of Amyloid- $\beta$  Plaques in Alzheimer’s Disease. *J. Med. Chem.* **2015**, *58*, 6972–6983. [[CrossRef](#)] [[PubMed](#)]
71. Fu, H.; Tu, P.; Zhao, L.; Dai, J.; Liu, B.; Cui, M. Amyloid- $\beta$  Deposits Target Efficient Near-Infrared Fluorescent Probes: Synthesis, in Vitro Evaluation, and in Vivo Imaging. *Anal. Chem.* **2016**, *88*, 1944–1950. [[CrossRef](#)] [[PubMed](#)]
72. Cui, M.; Ono, M.; Watanabe, H.; Kimura, H.; Liu, B.; Saji, H. Smart Near-Infrared Fluorescence Probes with Donor–Acceptor Structure for in Vivo Detection of  $\beta$ -Amyloid Deposits. *J. Am. Chem. Soc.* **2014**, *136*, 3388–3394. [[CrossRef](#)] [[PubMed](#)]
73. Kim, D.; Moon, H.; Baik, S.H.; Singha, S.; Jun, Y.W.; Wang, T.; Kim, K.H.; Park, B.S.; Jung, J.; Mook-Jung, I.; et al. Two-Photon Absorbing Dyes with Minimal Autofluorescence in Tissue Imaging: Application to in Vivo Imaging of Amyloid- $\beta$  Plaques with a Negligible Background Signal. *J. Am. Chem. Soc.* **2015**, *137*, 6781–6789. [[CrossRef](#)] [[PubMed](#)]
74. Nicole, O.; Hadzibegovic, S.; Gajda, J.; Bontempi, B.; Bem, T.; Meyrand, P. Soluble Amyloid Beta Oligomers Block the Learning-Induced Increase in Hippocampal Sharp Wave-Ripple Rate and Impair Spatial Memory Formation. *Sci. Rep.* **2016**, *6*, 22728. [[CrossRef](#)] [[PubMed](#)]
75. Larson, M.E.; Lesné, S.E. Soluble A $\beta$  Oligomer Production and Toxicity. *J. Neurochem.* **2012**, *120* (Suppl. 1), 125–139. [[CrossRef](#)] [[PubMed](#)]
76. Zhang, X.; Tian, Y.; Zhang, C.; Tian, X.; Ross, A.W.; Moir, R.D.; Sun, H.; Tanzi, R.E.; Moore, A.; Ran, C. Near-Infrared Fluorescence Molecular Imaging of Amyloid Beta Species and Monitoring Therapy in Animal Models of Alzheimer’s Disease. *Proc. Natl. Acad. Sci. USA* **2015**, *112*, 9734–9739. [[CrossRef](#)] [[PubMed](#)]
77. Teoh, C.L.; Su, D.; Sahu, S.; Yun, S.-W.; Drummond, E.; Prelli, F.; Lim, S.; Cho, S.; Ham, S.; Wisniewski, T.; et al. Chemical Fluorescent Probe for Detection of A $\beta$  Oligomers. *J. Am. Chem. Soc.* **2015**, *137*, 13503–13509. [[CrossRef](#)] [[PubMed](#)]
78. Jameson, L.P.; Dzyuba, S.V. Aza-BODIPY: Improved Synthesis and Interaction with Soluble A $\beta$ 1–42 Oligomers. *Bioorganic Med. Chem. Lett.* **2013**, *23*, 1732–1735. [[CrossRef](#)] [[PubMed](#)]
79. Yang, J.; Zeng, F.; Li, X.; Ran, C.; Xu, Y.; Li, Y. Highly Specific Detection of A $\beta$  Oligomers in Early Alzheimer’s Disease by a near-Infrared Fluorescent Probe with a “V-Shaped” Spatial Conformation. *Chem. Commun.* **2020**, *56*, 583–586. [[CrossRef](#)]
80. Li, H.; Wang, J.; Li, Y.; Chen, X.; Zhang, W.; Zhao, Y.; Liu, G.; Pan, J. Detection of A $\beta$  Oligomers in Early Alzheimer’s Disease Diagnose by in Vivo NIR-II Fluorescence Imaging. *Sens. Actuators B Chem.* **2022**, *358*, 131481. [[CrossRef](#)]
81. Li, Y.; Xu, D.; Sun, A.; Ho, S.-L.; Poon, C.-Y.; Chan, H.-N.; Ng, O.T.W.; Yung, K.K.L.; Yan, H.; Li, H.-W.; et al. Fluoro-Substituted Cyanine for Reliable in Vivo Labelling of Amyloid- $\beta$  Oligomers and Neuroprotection against Amyloid- $\beta$  Induced Toxicity. *Chem. Sci.* **2017**, *8*, 8279–8284. [[CrossRef](#)]
82. Weingarten, M.D.; Lockwood, A.H.; Hwo, S.Y.; Kirschner, M.W. A Protein Factor Essential for Microtubule Assembly. *Proc. Natl. Acad. Sci. USA* **1975**, *72*, 1858–1862. [[CrossRef](#)] [[PubMed](#)]
83. Goedert, M.; Wischik, C.M.; Crowther, R.A.; Walker, J.E.; Klug, A. Cloning and Sequencing of the cDNA Encoding a Core Protein of the Paired Helical Filament of Alzheimer Disease: Identification as the Microtubule-Associated Protein Tau. *Proc. Natl. Acad. Sci. USA* **1988**, *85*, 4051–4055. [[CrossRef](#)] [[PubMed](#)]
84. Deshpande, A.; Win, K.M.; Busciglio, J. Tau Isoform Expression and Regulation in Human Cortical Neurons. *FASEB J.* **2008**, *22*, 2357–2367. [[CrossRef](#)] [[PubMed](#)]
85. Guo, T.; Noble, W.; Hanger, D.P. Roles of Tau Protein in Health and Disease. *Acta Neuropathol.* **2017**, *133*, 665–704. [[CrossRef](#)] [[PubMed](#)]
86. Morris, J.K.; Honea, R.A.; Vidoni, E.D.; Swerdlow, R.H.; Burns, J.M. Is Alzheimer’s Disease a Systemic Disease? *Biochim. Biophys. Acta* **2014**, *1842*, 1340–1349. [[CrossRef](#)] [[PubMed](#)]
87. Tabeshmehr, P.; Eftekharpour, E. Tau: One Protein, So Many Diseases. *Biology* **2023**, *12*, 244. [[CrossRef](#)] [[PubMed](#)]
88. Wang, J.-Z.; Liu, F. Microtubule-Associated Protein Tau in Development, Degeneration and Protection of Neurons. *Prog. Neurobiol.* **2008**, *85*, 148–175. [[CrossRef](#)]
89. Kolarova, M.; García-Sierra, F.; Bartos, A.; Ricny, J.; Ripova, D. Structure and Pathology of Tau Protein in Alzheimer Disease. *Int. J. Alzheimer’s Dis.* **2012**, *2012*, 731526. [[CrossRef](#)]



90. Crespo-Biel, N.; Theunis, C.; Van Leuven, F. Protein Tau: Prime Cause of Synaptic and Neuronal Degeneration in Alzheimer's Disease. *Int. J. Alzheimer's Dis.* **2012**, *2012*, 251426. [[CrossRef](#)]
91. Rajasekhar, K.; Govindaraju, T. Current Progress, Challenges and Future Prospects of Diagnostic and Therapeutic Interventions in Alzheimer's Disease. *RSC Adv.* **2018**, *8*, 23780–23804. [[CrossRef](#)] [[PubMed](#)]
92. Soeda, Y.; Takashima, A. New Insights Into Drug Discovery Targeting Tau Protein. *Front. Mol. Neurosci.* **2020**, *13*, 590896. [[CrossRef](#)] [[PubMed](#)]
93. Pinzi, L.; Tinivella, A.; Rastelli, G. Chemoinformatics Analyses of Tau Ligands Reveal Key Molecular Requirements for the Identification of Potential Drug Candidates against Tauopathies. *Molecules* **2021**, *26*, 5039. [[CrossRef](#)] [[PubMed](#)]
94. Giovannini, J.; Smeralda, W.; Jouanne, M.; Sopkova-de Oliveira Santos, J.; Catto, M.; Voisin-Chiret, A.S. Tau Protein Aggregation: Key Features to Improve Drug Discovery Screening. *Drug Discov. Today* **2022**, *27*, 1284–1297. [[CrossRef](#)]
95. VandeVrede, L.; Boxer, A.L.; Polydoro, M. Targeting Tau: Clinical Trials and Novel Therapeutic Approaches. *Neurosci. Lett.* **2020**, *731*, 134919. [[CrossRef](#)]
96. Robbins, M. Therapies for Tau-Associated Neurodegenerative Disorders: Targeting Molecules, Synapses, and Cells. *Neural Regen. Res.* **2023**, *18*, 2633–2637. [[CrossRef](#)] [[PubMed](#)]
97. Zhang, S.; Dong, H.; Bian, J.; Li, D.; Liu, C. Targeting Amyloid Proteins for Clinical Diagnosis of Neurodegenerative Diseases. *Fundam. Res.* **2023**, *3*, 505–519. [[CrossRef](#)]
98. Pinzi, L.; Bisi, N.; Sorbi, C.; Franchini, S.; Tonali, N.; Rastelli, G. Insights into the Structural Conformations of the Tau Protein in Different Aggregation Status. *Molecules* **2023**, *28*, 4544. [[CrossRef](#)]
99. Wesseling, H.; Mair, W.; Kumar, M.; Schlaffner, C.N.; Tang, S.; Beerepoot, P.; Fatou, B.; Guise, A.J.; Cheng, L.; Takeda, S.; et al. Tau PTM Profiles Identify Patient Heterogeneity and Stages of Alzheimer's Disease. *Cell* **2020**, *183*, 1699–1713.e13. [[CrossRef](#)]
100. Zhang, H.; Cao, Y.; Ma, L.; Wei, Y.; Li, H. Possible Mechanisms of Tau Spread and Toxicity in Alzheimer's Disease. *Front. Cell Dev. Biol.* **2021**, *9*, 707268. [[CrossRef](#)]
101. Zhang, Y.; Wu, K.-M.; Yang, L.; Dong, Q.; Yu, J.-T. Tauopathies: New Perspectives and Challenges. *Mol. Neurodegener.* **2022**, *17*, 28. [[CrossRef](#)]
102. Chang, H.-Y.; Sang, T.-K.; Chiang, A.-S. Untangling the Tauopathy for Alzheimer's Disease and Parkinsonism. *J. Biomed. Sci.* **2018**, *25*, 54. [[CrossRef](#)]
103. Wang, Y.T.; Edison, P. Tau Imaging in Neurodegenerative Diseases Using Positron Emission Tomography. *Curr. Neurol. Neurosci. Rep.* **2019**, *19*, 45. [[CrossRef](#)]
104. Villemagne, V.L.; Fodero-Tavoletti, M.T.; Masters, C.L.; Rowe, C.C. Tau Imaging: Early Progress and Future Directions. *Lancet Neurol.* **2015**, *14*, 114–124. [[CrossRef](#)]
105. Yeung, A.W.K.; Goto, T.K.; Leung, W.K. The Changing Landscape of Neuroscience Research, 2006–2015: A Bibliometric Study. *Front. Neurosci.* **2017**, *11*, 120. [[CrossRef](#)]
106. James, O.G.; Doraiswamy, P.M.; Borges-Neto, S. PET Imaging of Tau Pathology in Alzheimer's Disease and Tauopathies. *Front. Neurol.* **2015**, *6*, 38. [[CrossRef](#)] [[PubMed](#)]
107. Shin, J.; Kepe, V.; Barrio, J.R.; Small, G.W. The Merits of FDDNP-PET Imaging in Alzheimer's Disease. *J. Alzheimer's Dis.* **2011**, *26* (Suppl. 3), 135–145. [[CrossRef](#)] [[PubMed](#)]
108. Wood, H. Alzheimer Disease: [11C]PBB3--a New PET Ligand That Identifies Tau Pathology in the Brains of Patients with AD. *Nat. Rev. Neurol.* **2013**, *9*, 599. [[CrossRef](#)] [[PubMed](#)]
109. Maruyama, M.; Shimada, H.; Suhara, T.; Shinotoh, H.; Ji, B.; Maeda, J.; Zhang, M.-R.; Trojanowski, J.Q.; Lee, V.M.-Y.; Ono, M.; et al. Imaging of Tau Pathology in a Tauopathy Mouse Model and in Alzheimer Patients Compared to Normal Controls. *Neuron* **2013**, *79*, 1094–1108. [[CrossRef](#)] [[PubMed](#)]
110. Okamura, N.; Suemoto, T.; Furumoto, S.; Suzuki, M.; Shimadzu, H.; Akatsu, H.; Yamamoto, T.; Fujiwara, H.; Nemoto, M.; Maruyama, M.; et al. Quinoline and Benzimidazole Derivatives: Candidate Probes for in Vivo Imaging of Tau Pathology in Alzheimer's Disease. *J. Neurosci.* **2005**, *25*, 10857–10862. [[CrossRef](#)] [[PubMed](#)]
111. Fodero-Tavoletti, M.T.; Okamura, N.; Furumoto, S.; Mulligan, R.S.; Connor, A.R.; McLean, C.A.; Cao, D.; Rigopoulos, A.; Cartwright, G.A.; O'Keefe, G.; et al. 18F-THK523: A Novel in Vivo Tau Imaging Ligand for Alzheimer's Disease. *Brain* **2011**, *134*, 1089–1100. [[CrossRef](#)] [[PubMed](#)]
112. Harada, R.; Okamura, N.; Furumoto, S.; Tago, T.; Maruyama, M.; Higuchi, M.; Yoshikawa, T.; Arai, H.; Iwata, R.; Kudo, Y.; et al. Comparison of the Binding Characteristics of [18F]THK-523 and Other Amyloid Imaging Tracers to Alzheimer's Disease Pathology. *Eur. J. Nucl. Med. Mol. Imaging* **2013**, *40*, 125–132. [[CrossRef](#)] [[PubMed](#)]
113. Okamura, N.; Furumoto, S.; Harada, R.; Tago, T.; Yoshikawa, T.; Fodero-Tavoletti, M.; Mulligan, R.S.; Villemagne, V.L.; Akatsu, H.; Yamamoto, T.; et al. Novel 18F-Labeled Arylquinoline Derivatives for Noninvasive Imaging of Tau Pathology in Alzheimer Disease. *J. Nucl. Med.* **2013**, *54*, 1420–1427. [[CrossRef](#)] [[PubMed](#)]
114. Villemagne, V.L.; Furumoto, S.; Fodero-Tavoletti, M.T.; Mulligan, R.S.; Hodges, J.; Harada, R.; Yates, P.; Piguet, O.; Pejoska, S.; Doré, V.; et al. In Vivo Evaluation of a Novel Tau Imaging Tracer for Alzheimer's Disease. *Eur. J. Nucl. Med. Mol. Imaging* **2014**, *41*, 816–826. [[CrossRef](#)] [[PubMed](#)]
115. Okamura, N.; Furumoto, S.; Fodero-Tavoletti, M.T.; Mulligan, R.S.; Harada, R.; Yates, P.; Pejoska, S.; Kudo, Y.; Masters, C.L.; Yanai, K.; et al. Non-Invasive Assessment of Alzheimer's Disease Neurofibrillary Pathology Using 18F-THK5105 PET. *Brain* **2014**, *137*, 1762–1771. [[CrossRef](#)] [[PubMed](#)]

116. Harada, R.; Okamura, N.; Furumoto, S.; Furukawa, K.; Ishiki, A.; Tomita, N.; Hiraoka, K.; Watanuki, S.; Shidahara, M.; Miyake, M.; et al. [<sup>18</sup>F]THK-5117 PET for Assessing Neurofibrillary Pathology in Alzheimer's Disease. *Eur. J. Nucl. Med. Mol. Imaging* **2015**, *42*, 1052–1061. [[CrossRef](#)] [[PubMed](#)]
117. Harada, R.; Okamura, N.; Furumoto, S.; Furukawa, K.; Ishiki, A.; Tomita, N.; Tago, T.; Hiraoka, K.; Watanuki, S.; Shidahara, M.; et al. 18F-THK5351: A Novel PET Radiotracer for Imaging Neurofibrillary Pathology in Alzheimer Disease. *J. Nucl. Med.* **2016**, *57*, 208–214. [[CrossRef](#)] [[PubMed](#)]
118. Commissioner, O. Of the FDA Approves First Drug to Image Tau Pathology in Patients Being Evaluated for Alzheimer's Disease. Available online: <https://www.fda.gov/news-events/press-announcements/fda-approves-first-drug-image-tau-pathology-patients-being-evaluated-alzheimers-disease> (accessed on 25 November 2023).
119. Barthel, H. First Tau PET Tracer Approved: Toward Accurate In Vivo Diagnosis of Alzheimer Disease. *J. Nucl. Med.* **2020**, *61*, 1409–1410. [[CrossRef](#)]
120. Tian, M.; Civelek, A.C.; Carrio, I.; Watanabe, Y.; Kang, K.W.; Murakami, K.; Garibotto, V.; Prior, J.O.; Barthel, H.; Zhou, R.; et al. International Consensus on the Use of Tau PET Imaging Agent 18F-Flortaucipir in Alzheimer's Disease. *Eur. J. Nucl. Med. Mol. Imaging* **2022**, *49*, 895–904. [[CrossRef](#)]
121. Lowe, V.J.; Lundt, E.S.; Albertson, S.M.; Min, H.-K.; Fang, P.; Przybelski, S.A.; Senjem, M.L.; Schwarz, C.G.; Kantarci, K.; Boeve, B.; et al. Tau-Positron Emission Tomography Correlates with Neuropathology Findings. *Alzheimer's Dement.* **2020**, *16*, 561–571. [[CrossRef](#)]
122. Xia, C.-F.; Arteaga, J.; Chen, G.; Gangadharmath, U.; Gomez, L.F.; Kasi, D.; Lam, C.; Liang, Q.; Liu, C.; Mocharla, V.P.; et al. [(18)F]T807, a Novel Tau Positron Emission Tomography Imaging Agent for Alzheimer's Disease. *Alzheimer's Dement.* **2013**, *9*, 666–676. [[CrossRef](#)] [[PubMed](#)]
123. Marquié, M.; Normandin, M.D.; Vanderburg, C.R.; Costantino, I.M.; Bien, E.A.; Rycyna, L.G.; Klunk, W.E.; Mathis, C.A.; Ikononovic, M.D.; Debnath, M.L.; et al. Validating Novel Tau Positron Emission Tomography Tracer [F-18]-AV-1451 (T807) on Postmortem Brain Tissue. *Ann. Neurol.* **2015**, *78*, 787–800. [[CrossRef](#)]
124. Fleisher, A.S.; Pontecorvo, M.J.; Devous, M.D.; Lu, M.; Arora, A.K.; Truocchio, S.P.; Aldea, P.; Flitter, M.; Locascio, T.; Devine, M.; et al. Positron Emission Tomography Imaging With [18F]Flortaucipir and Postmortem Assessment of Alzheimer Disease Neuropathologic Changes. *JAMA Neurol.* **2020**, *77*, 829–839. [[CrossRef](#)]
125. Vermeiren, C.; Motte, P.; Viot, D.; Mairet-Coello, G.; Courade, J.-P.; Citron, M.; Mercier, J.; Hannestad, J.; Gillard, M. The Tau Positron-Emission Tomography Tracer AV-1451 Binds with Similar Affinities to Tau Fibrils and Monoamine Oxidases. *Mov. Disord.* **2018**, *33*, 273–281. [[CrossRef](#)]
126. Cassinelli Petersen, G.; Roytman, M.; Chiang, G.C.; Li, Y.; Gordon, M.L.; Franceschi, A.M. Overview of Tau PET Molecular Imaging. *Curr. Opin. Neurol.* **2022**, *35*, 230–239. [[CrossRef](#)]
127. Brendel, M.; Schönecker, S.; Höglinger, G.; Lindner, S.; Havla, J.; Blautzik, J.; Sauerbeck, J.; Rohrer, G.; Zach, C.; Vettermann, F.; et al. [18F]-THK5351 PET Correlates with Topology and Symptom Severity in Progressive Supranuclear Palsy. *Front. Aging Neurosci.* **2018**, *9*, 440. [[CrossRef](#)]
128. Coakeley, S.; Cho, S.S.; Koshimori, Y.; Rusjan, P.; Harris, M.; Ghadery, C.; Kim, J.; Lang, A.E.; Wilson, A.; Houle, S.; et al. Positron Emission Tomography Imaging of Tau Pathology in Progressive Supranuclear Palsy. *J. Cereb. Blood Flow. Metab.* **2017**, *37*, 3150–3160. [[CrossRef](#)]
129. Leuzy, A.; Chiotis, K.; Lemoine, L.; Gillberg, P.-G.; Almkvist, O.; Rodriguez-Vieitez, E.; Nordberg, A. Tau PET Imaging in Neurodegenerative Tauopathies—Still a Challenge. *Mol. Psychiatry* **2019**, *24*, 1112–1134. [[CrossRef](#)] [[PubMed](#)]
130. Wolters, E.E.; Dodich, A.; Boccardi, M.; Corre, J.; Drzezga, A.; Hansson, O.; Nordberg, A.; Frisoni, G.B.; Garibotto, V.; Ossenkoppele, R. Clinical Validity of Increased Cortical Uptake of [18F]Flortaucipir on PET as a Biomarker for Alzheimer's Disease in the Context of a Structured 5-Phase Biomarker Development Framework. *Eur. J. Nucl. Med. Mol. Imaging* **2021**, *48*, 2097–2109. [[CrossRef](#)] [[PubMed](#)]
131. Harada, R.; Lerdsirisuk, P.; Shimizu, Y.; Yokoyama, Y.; Du, Y.; Kudo, K.; Ezura, M.; Ishikawa, Y.; Iwata, R.; Shidahara, M.; et al. Preclinical Characterization of the Tau PET Tracer [18F]SNFT-1: Comparison of Tau PET Tracers. *J. Nucl. Med.* **2023**, *64*, 1495–1501. [[CrossRef](#)] [[PubMed](#)]
132. Malarte, M.-L.; Gillberg, P.-G.; Kumar, A.; Bogdanovic, N.; Lemoine, L.; Nordberg, A. Discriminative Binding of Tau PET Tracers PI2620, MK6240 and RO948 in Alzheimer's Disease, Corticobasal Degeneration and Progressive Supranuclear Palsy Brains. *Mol. Psychiatry* **2023**, *28*, 1272–1283. [[CrossRef](#)] [[PubMed](#)]
133. Pascoal, T.A.; Mathotaarachchi, S.; Shin, M.; Benedet, A.L.; Mohades, S.; Wang, S.; Beaudry, T.; Kang, M.S.; Soucy, J.; Labbe, A.; et al. Synergistic Interaction between Amyloid and Tau Predicts the Progression to Dementia. *Alzheimer's Dement.* **2017**, *13*, 644–653. [[CrossRef](#)]
134. Mueller, A.; Bullich, S.; Barret, O.; Madonia, J.; Berndt, M.; Papin, C.; Perrotin, A.; Koglin, N.; Kroth, H.; Pfeifer, A.; et al. Tau PET Imaging with 18F-PI-2620 in Patients with Alzheimer Disease and Healthy Controls: A First-in-Humans Study. *J. Nucl. Med.* **2020**, *61*, 911–919. [[CrossRef](#)]
135. Leuzy, A.; Smith, R.; Ossenkoppele, R.; Santillo, A.; Borroni, E.; Klein, G.; Ohlsson, T.; Jögi, J.; Palmqvist, S.; Mattsson-Carlgrén, N.; et al. Diagnostic Performance of RO948 F 18 Tau Positron Emission Tomography in the Differentiation of Alzheimer Disease From Other Neurodegenerative Disorders. *JAMA Neurol.* **2020**, *77*, 955–965. [[CrossRef](#)] [[PubMed](#)]



136. Rowe, C.C.; Doré, V.; Krishnadas, N.; Burnham, S.; Lamb, F.; Mulligan, R.; Bozinovski, S.; Laws, S.; Tyrell, R.; Huang, K.; et al. Tau Imaging with 18F-MK6240 across the Alzheimer's Disease Spectrum. *medRxiv* **2022**. medRxiv:2022.02.13.22270894.
137. Xu, X.; Ruan, W.; Liu, F.; Gai, Y.; Liu, Q.; Su, Y.; Liang, Z.; Sun, X.; Lan, X. 18F-APN-1607 Tau Positron Emission Tomography Imaging for Evaluating Disease Progression in Alzheimer's Disease. *Front. Aging Neurosci.* **2022**, *13*, 789054. [[CrossRef](#)] [[PubMed](#)]
138. Merz, G.E.; Chalkley, M.J.; Tan, S.K.; Tse, E.; Lee, J.; Prusiner, S.B.; Paras, N.A.; DeGrado, W.F.; Southworth, D.R. Stacked Binding of a PET Ligand to Alzheimer's Tau Paired Helical Filaments. *Nat. Commun.* **2023**, *14*, 3048. [[CrossRef](#)] [[PubMed](#)]
139. Seidler, P.M.; Murray, K.A.; Boyer, D.R.; Ge, P.; Sawaya, M.R.; Hu, C.J.; Cheng, X.; Abskharon, R.; Pan, H.; DeTure, M.A.; et al. Structure-Based Discovery of Small Molecules That Disaggregate Alzheimer's Disease Tissue Derived Tau Fibrils in Vitro. *Nat. Commun.* **2022**, *13*, 5451. [[CrossRef](#)] [[PubMed](#)]
140. Leuzy, A.; Smith, R.; Cullen, N.C.; Strandberg, O.; Vogel, J.W.; Binette, A.P.; Borroni, E.; Janelidze, S.; Ohlsson, T.; Jögi, J.; et al. Biomarker-Based Prediction of Longitudinal Tau Positron Emission Tomography in Alzheimer Disease. *JAMA Neurol.* **2022**, *79*, 149–158. [[CrossRef](#)]
141. Rojo, L.E.; Alzate-Morales, J.; Saavedra, I.N.; Davies, P.; Maccioni, R.B. Selective Interaction of Lansoprazole and Astemizole with Tau Polymers: Potential New Clinical Use in Diagnosis of Alzheimer's Disease. *J. Alzheimer's Dis.* **2010**, *19*, 573–589. [[CrossRef](#)] [[PubMed](#)]
142. Yeo, S.K.; Shepelytskyi, Y.; Grynko, V.; Albert, M.S. Molecular Imaging of Fluorinated Probes for Tau Protein and Amyloid- $\beta$  Detection. *Molecules* **2020**, *25*, 3413. [[CrossRef](#)]
143. Ni, R. Magnetic Resonance Imaging in Tauopathy Animal Models. *Front. Aging Neurosci.* **2022**, *13*, 791679. [[CrossRef](#)] [[PubMed](#)]
144. Hane, F.T.; Robinson, M.; Lee, B.Y.; Bai, O.; Leonenko, Z.; Albert, M.S. Recent Progress in Alzheimer's Disease Research, Part 3: Diagnosis and Treatment. *J. Alzheimer's Dis.* **2017**, *57*, 645–665. [[CrossRef](#)] [[PubMed](#)]
145. Reitz, C.; Mayeux, R. Alzheimer Disease: Epidemiology, Diagnostic Criteria, Risk Factors and Biomarkers. *Biochem. Pharmacol.* **2014**, *88*, 640–651. [[CrossRef](#)] [[PubMed](#)]
146. Frisoni, G.B.; Fox, N.C.; Jack, C.R.; Scheltens, P.; Thompson, P.M. The Clinical Use of Structural MRI in Alzheimer Disease. *Nat. Rev. Neurol.* **2010**, *6*, 67–77. [[CrossRef](#)] [[PubMed](#)]
147. Higuchi, M.; Iwata, N.; Matsuba, Y.; Sato, K.; Sasamoto, K.; Saido, T.C. 19F and 1H MRI Detection of Amyloid  $\beta$  Plaques In Vivo. *Nat. Neurosci.* **2005**, *8*, 527–533. [[CrossRef](#)] [[PubMed](#)]
148. Amatsubo, T.; Yanagisawa, D.; Morikawa, S.; Taguchi, H.; Tooyama, I. Amyloid Imaging Using High-Field Magnetic Resonance. *Magn. Reson. Med. Sci.* **2010**, *9*, 95–99. [[CrossRef](#)]
149. Yanagisawa, D.; Ibrahim, N.F.; Taguchi, H.; Morikawa, S.; Kato, T.; Hirao, K.; Shirai, N.; Sogabe, T.; Tooyama, I. Fluorine-19 Magnetic Resonance Imaging Probe for the Detection of Tau Pathology in Female RTg4510 Mice. *J. Neurosci. Res.* **2018**, *96*, 841–851. [[CrossRef](#)]
150. Badachhane, A.; Parekh, P.A.; Mu, Q.; Bhavane, R.; Srivastava, M.; Stupin, I.; Bhandari, P.; Devkota, L.; Tanifum, E.; Ghaghada, K.; et al. A Novel MRI Contrast Agent for Identifying Hyperphosphorylated Neurons as a Marker of Future Tau Pathology. *Alzheimer's Dement.* **2020**, *16*, e041080. [[CrossRef](#)]
151. Yamanakkanavar, N.; Choi, J.Y.; Lee, B. MRI Segmentation and Classification of Human Brain Using Deep Learning for Diagnosis of Alzheimer's Disease: A Survey. *Sensors* **2020**, *20*, 3243. [[CrossRef](#)]
152. Li, C.; Liu, M.; Xia, J.; Mei, L.; Yang, Q.; Shi, F.; Zhang, H.; Shen, D. Predicting Brain Amyloid- $\beta$  PET Phenotypes with Graph Convolutional Networks Based on Functional MRI and Multi-Level Functional Connectivity. *J. Alzheimer's Dis.* **2021**, *86*, 1679–1693. [[CrossRef](#)] [[PubMed](#)]
153. Ten Kate, M.; Redolfi, A.; Peira, E.; Bos, I.; Vos, S.J.; Vandenberghe, R.; Gabel, S.; Schaefferbeke, J.; Scheltens, P.; Blin, O.; et al. MRI Predictors of Amyloid Pathology: Results from the EMIF-AD Multimodal Biomarker Discovery Study. *Alzheimer's Res. Ther.* **2018**, *10*, 100. [[CrossRef](#)]
154. Kang, S.H.; Cheon, B.K.; Kim, J.-S.; Jang, H.; Kim, H.J.; Park, K.W.; Noh, Y.; Lee, J.S.; Ye, B.S.; Na, D.L.; et al. Machine Learning for the Prediction of Amyloid Positivity in Amnesic Mild Cognitive Impairment. *J. Alzheimer's Dis.* **2021**, *80*, 143–157. [[CrossRef](#)]
155. Lew, C.O.; Zhou, L.; Mazurowski, M.A.; Doraiswamy, P.M.; Petrella, J.R.; Alzheimer's Disease Neuroimaging Initiative. MRI-Based Deep Learning Assessment of Amyloid, Tau, and Neurodegeneration Biomarker Status across the Alzheimer Disease Spectrum. *Radiology* **2023**, *309*, e222441. [[CrossRef](#)]
156. Barghorn, S.; Biernat, J.; Mandelkow, E. Purification of Recombinant Tau Protein and Preparation of Alzheimer-Paired Helical Filaments in Vitro. *Methods Mol. Biol.* **2005**, *299*, 35–51. [[CrossRef](#)] [[PubMed](#)]
157. Sui, D.; Liu, M.; Kuo, M.-H. In Vitro Aggregation Assays Using Hyperphosphorylated Tau Protein. *J. Vis. Exp.* **2015**, *95*, e51537. [[CrossRef](#)]
158. Elbatrawy, A.A.; Hyeon, S.J.; Yue, N.; Osman, E.E.A.; Choi, S.H.; Lim, S.; Kim, Y.K.; Ryu, H.; Cui, M.; Nam, G. "Turn-On" Quinoline-Based Fluorescent Probe for Selective Imaging of Tau Aggregates in Alzheimer's Disease: Rational Design, Synthesis, and Molecular Docking. *ACS Sens.* **2021**, *6*, 2281–2289. [[CrossRef](#)] [[PubMed](#)]
159. Ding, H.; Li, Z.; Luo, K.; Gong, Q.; Tian, X. Application of Biomarker-Derived Fluorescent Probes for the Detection of Alzheimer's Disease. *TrAC Trends Anal. Chem.* **2023**, *169*, 117369. [[CrossRef](#)]
160. Verwilst, P.; Kim, H.S.; Kim, S.; Kang, C.; Kim, J.S. Shedding Light on Tau Protein Aggregation: The Progress in Developing Highly Selective Fluorophores. *Chem. Soc. Rev.* **2018**, *47*, 2249–2265. [[CrossRef](#)]

161. Verwilst, P.; Kim, H.-R.; Seo, J.; Sohn, N.-W.; Cha, S.-Y.; Kim, Y.; Maeng, S.; Shin, J.-W.; Kwak, J.H.; Kang, C.; et al. Rational Design of in Vivo Tau Tangle-Selective Near-Infrared Fluorophores: Expanding the BODIPY Universe. *J. Am. Chem. Soc.* **2017**, *139*, 13393–13403. [[CrossRef](#)]
162. Zhao, Y.; Tietz, O.; Kuan, W.-L.; Haji-Dheere, A.K.; Thompson, S.; Vallin, B.; Ronchi, E.; Tóth, G.; Klenerman, D.; Aigbirio, F.I. A Fluorescent Molecular Imaging Probe with Selectivity for Soluble Tau Aggregated Protein. *Chem. Sci.* **2020**, *11*, 4773–4778. [[CrossRef](#)]
163. Åslund, A.; Sigurdson, C.J.; Klingstedt, T.; Grathwohl, S.; Bolmont, T.; Dickstein, D.L.; Glimsdal, E.; Prokop, S.; Lindgren, M.; Konradsson, P.; et al. Novel Pentameric Thiophene Derivatives for in Vitro and in Vivo Optical Imaging of a Plethora of Protein Aggregates in Cerebral Amyloidoses. *ACS Chem. Biol.* **2009**, *4*, 673–684. [[CrossRef](#)]
164. Oh, Y.; Lee, T.; Kim, M.K.; Chong, Y. Thiophene- $\pi$ -Cyanoacetamides Show Intense and Tau-Selective Turn-on Fluorescence in the Near-Infrared Region. *Bull. Korean Chem. Soc.* **2021**, *42*, 1285–1288. [[CrossRef](#)]
165. Soloperto, A.; Quaglio, D.; Baiocco, P.; Romeo, I.; Mori, M.; Ardini, M.; Presutti, C.; Sannino, I.; Ghirga, S.; Iazzetti, A.; et al. Rational Design and Synthesis of a Novel BODIPY-Based Probe for Selective Imaging of Tau Tangles in Human iPSC-Derived Cortical Neurons. *Sci. Rep.* **2022**, *12*, 5257. [[CrossRef](#)]
166. Fields, C.R.; Bengoa-Vergniory, N.; Wade-Martins, R. Targeting Alpha-Synuclein as a Therapy for Parkinson's Disease. *Front. Mol. Neurosci.* **2019**, *12*, 299. [[CrossRef](#)]
167. Shvadchak, V.V.; Afitska, K.; Yushchenko, D.A. Inhibition of  $\alpha$ -Synuclein Amyloid Fibril Elongation by Blocking Fibril Ends. *Angew. Chem. Int. Ed.* **2018**, *57*, 5690–5694. [[CrossRef](#)]
168. Veys, L.; Vandenabeele, M.; Ortuño-Lizarán, I.; Baekelandt, V.; Cuenca, N.; Moons, L.; De Groef, L. Retinal  $\alpha$ -Synuclein Deposits in Parkinson's Disease Patients and Animal Models. *Acta Neuropathol.* **2019**, *137*, 379–395. [[CrossRef](#)]
169. Deeg, A.A.; Reiner, A.M.; Schmidt, F.; Schueder, F.; Ryazanov, S.; Ruf, V.C.; Giller, K.; Becker, S.; Leonov, A.; Griesinger, C.; et al. Anle138b and Related Compounds Are Aggregation Specific Fluorescence Markers and Reveal High Affinity Binding to  $\alpha$ -Synuclein Aggregates. *Biochim. Acta* **2015**, *1850*, 1884–1890. [[CrossRef](#)]
170. Martinez Hernandez, A.; Urbanke, H.; Gillman, A.L.; Lee, J.; Ryazanov, S.; Agbemenyah, H.Y.; Benito, E.; Jain, G.; Kaurani, L.; Grigorian, G.; et al. The Diphenylpyrazole Compound Anle138b Blocks A $\beta$  Channels and Rescues Disease Phenotypes in a Mouse Model for Amyloid Pathology. *EMBO Mol. Med.* **2018**, *10*, 32–47. [[CrossRef](#)] [[PubMed](#)]
171. Wagner, J.; Krauss, S.; Shi, S.; Ryazanov, S.; Steffen, J.; Miklitz, C.; Leonov, A.; Kleinknecht, A.; Göricke, B.; Weishaupt, J.H.; et al. Reducing Tau Aggregates with Anle138b Delays Disease Progression in a Mouse Model of Tauopathies. *Acta Neuropathol.* **2015**, *130*, 619–631. [[CrossRef](#)] [[PubMed](#)]
172. Watanabe, H.; Ono, M.; Ariyoshi, T.; Katayanagi, R.; Saji, H. Novel Benzothiazole Derivatives as Fluorescent Probes for Detection of  $\beta$ -Amyloid and  $\alpha$ -Synuclein Aggregates. *ACS Chem. Neurosci.* **2017**, *8*, 1656–1662. [[CrossRef](#)] [[PubMed](#)]
173. Li, B.; Ge, P.; Murray, K.A.; Sheth, P.; Zhang, M.; Nair, G.; Sawaya, M.R.; Shin, W.S.; Boyer, D.R.; Ye, S.; et al. Cryo-EM of Full-Length  $\alpha$ -Synuclein Reveals Fibril Polymorphs with a Common Structural Kernel. *Nat. Commun.* **2018**, *9*, 3609. [[CrossRef](#)]
174. Alam, P.; Bousset, L.; Melki, R.; Otzen, D.E.  $\alpha$ -Synuclein Oligomers and Fibrils: A Spectrum of Species, a Spectrum of Toxicities. *J. Neurochem.* **2019**, *150*, 522–534. [[CrossRef](#)]
175. Zeng, Q.; Cui, M. Current Progress in the Development of Probes for Targeting  $\alpha$ -Synuclein Aggregates. *ACS Chem. Neurosci.* **2022**, *13*, 552–571. [[CrossRef](#)]
176. Bagchi, D.P.; Yu, L.; Perlmutter, J.S.; Xu, J.; Mach, R.H.; Tu, Z.; Kotzbauer, P.T. Binding of the Radioligand SIL23 to  $\alpha$ -Synuclein Fibrils in Parkinson Disease Brain Tissue Establishes Feasibility and Screening Approaches for Developing a Parkinson Disease Imaging Agent. *PLoS ONE* **2013**, *8*, e55031. [[CrossRef](#)]
177. Korat, S.; Bidesi, N.S.R.; Bonanno, F.; Di Nanni, A.; Hoàng, A.N.N.; Herfert, K.; Maurer, A.; Battisti, U.M.; Bowden, G.D.; Thonon, D.; et al. Alpha-Synuclein PET Tracer Development—An Overview about Current Efforts. *Pharmaceuticals* **2021**, *14*, 847. [[CrossRef](#)]
178. Chu, W.; Zhou, D.; Gaba, V.; Liu, J.; Li, S.; Peng, X.; Xu, J.; Dhavale, D.; Bagchi, D.P.; d'Avignon, A.; et al. Design, Synthesis, and Characterization of 3-(Benzylidene)Indolin-2-One Derivatives as Ligands for  $\alpha$ -Synuclein Fibrils. *J. Med. Chem.* **2015**, *58*, 6002–6017. [[CrossRef](#)] [[PubMed](#)]
179. Ono, M.; Doi, Y.; Watanabe, H.; Ihara, M.; Ozaki, A.; Saji, H. Structure–Activity Relationships of Radioiodinated Diphenyl Derivatives with Different Conjugated Double Bonds as Ligands for  $\alpha$ -Synuclein Aggregates. *RSC Adv.* **2016**, *6*, 44305–44312. [[CrossRef](#)]
180. Verdurand, M.; Levigoureux, E.; Zeinyeh, W.; Berthier, L.; Mendjel-Herda, M.; Cadarossanesaib, F.; Bouillot, C.; Iecker, T.; Terreux, R.; Lancelot, S.; et al. In Silico, in Vitro, and in Vivo Evaluation of New Candidates for  $\alpha$ -Synuclein PET Imaging. *Mol. Pharm.* **2018**, *15*, 3153–3166. [[CrossRef](#)]
181. Maurer, A.; Leonov, A.; Ryazanov, S.; Herfert, K.; Kuebler, L.; Buss, S.; Schmidt, F.; Weckbecker, D.; Linder, R.; Bender, D.; et al. <sup>11</sup>C Radiolabeling of Anle253b: A Putative PET Tracer for Parkinson's Disease That Binds to  $\alpha$ -Synuclein Fibrils in Vitro and Crosses the Blood-Brain Barrier. *ChemMedChem* **2020**, *15*, 411–415. [[CrossRef](#)] [[PubMed](#)]

182. Kuebler, L.; Buss, S.; Leonov, A.; Ryazanov, S.; Schmidt, F.; Maurer, A.; Weckbecker, D.; Landau, A.M.; Lillethorup, T.P.; Bleher, D.; et al. [11C]MODAG-001-towards a PET Tracer Targeting  $\alpha$ -Synuclein Aggregates. *Eur. J. Nucl. Med. Mol. Imaging* **2021**, *48*, 1759–1772. [[CrossRef](#)] [[PubMed](#)]
183. Kaide, S.; Watanabe, H.; Shimizu, Y.; Iikuni, S.; Nakamoto, Y.; Hasegawa, M.; Itoh, K.; Ono, M. Identification and Evaluation of Bisquinoline Scaffold as a New Candidate for  $\alpha$ -Synuclein-PET Imaging. *ACS Chem. Neurosci.* **2020**, *11*, 4254–4261. [[CrossRef](#)] [[PubMed](#)]

**Disclaimer/Publisher’s Note:** The statements, opinions and data contained in all publications are solely those of the individual author(s) and contributor(s) and not of MDPI and/or the editor(s). MDPI and/or the editor(s) disclaim responsibility for any injury to people or property resulting from any ideas, methods, instructions or products referred to in the content.